Journal of Natural Gas Science and Engineering 26 (2015) 1091–1106

Contents lists available at ScienceDirect

Journal of Natural Gas Science and Engineering

journal homepage: www.elsevier.com/locate/jngse

Characterization of water-containing reservoir oil using an EOS for steam injection processes

Arun Venkat Venkatramani, Ryosuke Okuno*

School of Mining and Petroleum Engineering, University of Alberta, 6-281 Donadeo Innovation Center for Engineering, Edmonton, Alberta T6G 1H9, Canada

ARTICLE INFO

Article history:
Received 21 February 2015
Received in revised form
30 June 2015
Accepted 23 July 2015
Available online 26 July 2015

Keywords:
Thermal oil recovery
Steam-assisted gravity drainage
Water solubilities
Equation of state
Binary interaction parameters

ABSTRACT

Experimental results in the literature indicate that the water solubility in the oleic (L) phase (x_{wL}) can be high at reservoir conditions in thermal oil recovery processes. However, the effect of x_{wL} on oil recovery has not been fully understood, especially for steam-assisted gravity drainage (SAGD) for in-situ bitumen recovery. This research presents a framework for reliable characterization of water/reservoir–oil mixtures for numerical simulation of steam injection processes. The Peng–Robinson equation of state (PR EOS) is used with the van der Waals mixing rules.

A new correlation is developed for binary interaction parameters (BIPs) for water with n-alkanes. Unlike previously proposed BIP values, the new correlation is based on optimization of three-phase predictions for water/n-alkane binaries, including upper critical endpoints (UCEPs). In the characterization method proposed for water-containing reservoir oil, the developed correlation serves as the well-defined upper limit for BIPs of water with hydrocarbon components. A SAGD simulation case study for Athabasca bitumen shows that bitumen recovery can be substantially affected by x_{wL} through the L-phase mobility. The characterization method developed in this research can be used with at least one measured x_{wL} value for a reliable phase-behavior model for steam injection simulation.

1. Introduction

Steam injection is a widely-used method for in-situ recovery of heavy oil and bitumen (Prats, 1982). In general, the primary mechanism of oil recovery in steam injection is the enhancement of the oleic (L) phase mobility owing to the heat transfer near thermal fronts. Although only a fraction of the injected heat can reside in the L phase, steam injection can be practical because the viscosity of heavy oil and bitumen is highly sensitive to temperature (Ahmed, 2006; Lake, 1989). For example, experimental data for an Athabasca bitumen showed that the viscosity was reduced by three orders of magnitude from 285 K to 393 K (Mehrotra and Svrcek, 1986).

Steam-assisted gravity drainage (SAGD) is an important application of steam injection, and is the most widely implemented method for in-situ bitumen recovery (Butler, 1994, 2001; Keshavarz et al., 2014a). In SAGD, steam is injected into a bitumen reservoir through a horizontal well. The injected steam forms a steam chamber and releases its latent heat at the chamber edge. The heated oil and condensed hot water drain to another horizontal well, which is located 5–10 m below and parallel to the injection well.

Flow of fluid and energy is coupled with multiphase behavior of water–hydrocarbon mixtures in steam injection, including SAGD. The complex interplay of flow with phase behavior affects the in-situ propagation of heat and components under gravity and reservoir heterogeneity. Due to the complexity, numerical reservoir simulation is commonly used to design steam injection processes. Such simulations should be conducted with reliable phase-behavior representation over a wide range of temperature from the initial reservoir temperature to the steam temperature at an operating pressure (e.g., from 285 K to 500 K).

Mixtures of water and hydrocarbons exhibit complex multiphase behavior consisting of the L, vapor (V), and aqueous (W) phases. In particular, the water dissolution in the L phase (x_{wL}) can be substantial at temperatures relevant to steam injection processes (Griswold and Kasch, 1942; Glandt and Chapman, 1995; Amani et al., 2013a, 2013b). For example, the x_{wL} measured on the three-phase curve for the water/n-C_{20} binary is approximately

* Corresponding author.
E-mail address: rokuno@ualberta.ca (R. Okuno).

http://dx.doi.org/10.1016/j.jngse.2015.07.036
1875-5100/

23.68 mol% at 523.15 K (Skripka, 1979). Experimental results for water binaries with n-alkanes have given a systematic set of data to understand the water solubility behavior (Reamer et al., 1944; Kobayashi and Katz, 1953; Skripka, 1979; Tsonopoulos and Wilson, 1983; Heidman et al., 1985; Economou et al., 1997; Shinta and Firoozabadi, 1997; Tsonopoulos, 1999; Maczynski et al., 2005; Shaw et al., 2005, 2006a, 2006b). The heaviest n-alkane for which x_{wL} data are available in the literature is n-C_{20} (Skripka, 1979; Shinta and Firoozabadi, 1997), to the best of our knowledge. An overview of the experimental multiphase behavior of water/n-alkane binaries is presented in Section S1 of Supplementary Material.

Results of Griswold and Kasch (1942), Tsonopoulos and Wilson (1983), and Heidman et al. (1985) show that x_{wL} becomes even more significant as the L phase becomes more aromatic, which is the case with bitumen. Glandt and Chapman (1995) and Amani et al. (2013a, 2013b) presented x_{wL} values measured for heavy oils and bitumens. Their results indicate that x_{wL} can be as high as 55 mol% at 550 K. In spite of these experimental data presented in the literature, current practice does not satisfactorily represent the multiphase behavior of water/hydrocarbon mixtures, especially x_{wL}, in thermal reservoir flow simulation (Keshavarz et al., 2014a, 2014b, 2015). This is likely because no framework has been established for characterization of water/reservoir–oil mixtures using an equation of state (EOS).

Glandt and Chapman (1995) and Amani et al. (2013a, 2013b) accentuated the potential importance of x_{wL} in the design of thermal recovery operations for heavy-oil and bitumen recovery. However, the extent of its significance in subsurface processes was not ascertained within their papers. Luo and Barrufet (2005) used a compositional thermal simulator to show that oil recovery in steam injection was calculated to be more efficient if x_{wL} was considered. This was primarily because the water dissolution made the L-phase viscosity lower in their reservoir simulation. This is consistent with Glandt and Chapman (1995), who observed in their experiments that the L-phase viscosity was reduced by the dissolved water at elevated temperatures. However, Luo and Barrufet's simulation cases were presented only for relatively light oils of 20°API and 35°API (specific gravities of 0.934 and 0.850, respectively). It is uncertain how significant it can be to properly consider the water dissolution in the L phase in flow simulation of thermal bitumen recovery. This is an important engineering question, considering the high aromaticity of the L phase and high operating temperature in SAGD (Amani et al., 2013a, 2013b).

There are two main objectives in the current research. One is to develop a reliable method for characterizing multiphase compositional behavior of water-containing reservoir oil by use of the Peng–Robinson (PR) EOS (Peng and Robinson, 1976a; Robinson and Peng, 1978) with the van der Waals mixing rules. The interaction between water and hydrocarbon pseudo components is characterized by perturbation from the interaction between water and n-alkanes that is developed in this research. The other objective of this research is to investigate the importance of properly considering x_{wL} in simulation of thermal bitumen recovery.

Section 2 presents the development of a new correlation for binary interaction parameters (BIPs) for water with n-alkanes. This correlation will be shown to be useful for characterizing water-containing reservoir oils with available x_{wL} data. In Section 3, the significance of the proposed characterization method will be demonstrated in simulation case studies for bitumen recovery in SAGD. To the best of our knowledge, this is the first time the effect of x_{wL} on thermal bitumen recovery is quantitatively studied and presented in the literature.

2. Characterization of water-containing reservoir oil

Reservoir oil contains a large number of components, most of which are non-identifiable. The non-identifiable heavy fractions are reported as single carbon number fractions and a lumped fraction (e.g., heptane-plus, or C_{7+}) from composition analysis. Therefore, reservoir oil is usually characterized by matching experimental phase-behavior data (e.g., liquid densities and saturation pressures) using an EOS with a few pseudo components (Pedersen et al., 2006; Whitson and Brulé, 2000). Reservoir oil characterization using a cubic EOS has been studied extensively in the literature, and is not the focus in this paper. Hence, reservoir oils that have been characterized by a published method (Kumar and Okuno, 2013, 2014) are used throughout this research.

The current research is concerned with reliable characterization of the interaction between reservoir oil and water for simulation of thermal oil recovery processes. The Peng–Robinson (PR) EOS (Appendix A) is used along with the van der Waals mixing rules because of its widespread usage in the petroleum industry.

In this section, BIPs for water with n-alkanes are optimized in terms of prediction of three-phase (L–V–W) curves. On the basis of the optimized values, a correlation is developed for water/n-alkane BIP with respect to n-alkane molecular weight (MW). The BIP correlation is then validated with various experimental data. After that, it is shown that the correlation gives a physically meaningful upper bound for BIP values for water with pseudo components when x_{wL} data for water-containing reservoir oils are matched.

2.1. New BIPs for water with n-alkanes

In this subsection, the BIPs for water with n-alkanes are optimized using the three-phase pressure–temperature (P–T) data points, including those for upper critical endpoints (UCEPs), reported in Brunner (1990) for water/n-alkanes binaries from C_3 through C_{36}. Water/n-alkane data are used not only because of their availability, but also because n-alkanes exhibit the limiting phase behavior in terms of aromaticity; that is, n-alkanes exhibit the least affinity towards water in comparison with aromatics and naphthenes (Tsonopoulos and Wilson, 1983; Heidman et al., 1985; Economou et al., 1997; Tsonopoulos, 1999).

Water/n-alkane binaries exhibit type III phase behavior, which can be further classified into types IIIa and IIIb. At the UCEP, the L and V phases become critical in the presence of the W phase for type IIIa binaries. The V and W phases become critical in the presence of the L phase at the UCEP for type IIIb binaries (see Section S1 of Supplementary Material).

T-x and P-x cross-sections at sub-UCEP conditions indicate that the phase compositions at three-phase conditions represent the boundary for the L–W/V–W and L–W/L–V phase transitions. That is, two-phase equilibria of water/n-alkane binaries are originated with three-phase behavior. The UCEP is the limiting three-phase behavior. Hence, it is important to find a proper set of BIPs for the PR EOS to be able to accurately represent water/n-alkane multiphase behavior.

Brunner (1990) presented data for 21 binaries, but data for the water/n-C_{26} binary are not used in the current optimization. This is because the UCEP for this binary was reported to be identical to that for the water/n-C_{28} binary, which caused a deviation from the overall trend. No explanation was given regarding this deviation. There are 213 data points on three-phase curves, out of which 20 data points are for UCEPs for 20 different binaries, all of which are used in the optimization.

The computational methods used for three-phase curves (including UCEPs) of water/n-alkane binaries are described in Section S2 of Supplementary Material. Three types of deviations are

considered in the BIP optimization as follows:

$$\Delta T_{3\varphi} = \left| T_{3\varphi}^{EOS}(P) - T_{3\varphi}^{Data}(P) \right| \quad (1)$$

$$\Delta T_{UCEP} = \left| T_{UCEP}^{EOS} - T_{UCEP}^{Data} \right| \quad (2)$$

$$\Delta P_{UCEP} = \left| P_{UCEP}^{EOS} - P_{UCEP}^{Data} \right|, \quad (3)$$

where superscripts "EOS" and "Data" indicate prediction from EOS and measured data, respectively. Subscripts "3φ" and "UCEP" indicate values for three-phase equilibrium and UCEP.

Experimental uncertainties associated with Brunner's measurements increase with increasing temperature and pressure. At temperatures higher than around 600 K, thermal decomposition of the n-alkanes can occur, which further contributes to the uncertainty. Hence, the optimization of the BIP in terms of the UCEP alone (Equations (2) and (3)) is insufficient. This necessitates the inclusion of Equation (1) as part of the optimization criteria.

In addition to Equations 1 through 3, the type of transition that occurs at the UCEP (i.e., type IIIa and type IIIb as described in Section S1 of Supplementary Material) is also considered when ascertaining the optimized BIP. For type IIIb systems, the asymptotic behavior of x_{wL} along the three-phase curves with respect to carbon number (CN) is properly preserved in the optimization.

The only adjustable parameter in the optimization for each binary is the BIP. The critical temperature and pressure (T_C and P_C) of water are 647.096 K and 220.64 bars, respectively (Wagner and Pruß, 2002). The acentric factor (ω) of water is 0.3433 on the basis of the vapor pressure correlation of Wagner and Pruß (2002). The API technical data book (Daubert and Danner, 1997) presents recommended values for T_C, P_C, and ω for n-alkanes up to n-C_{30}. Constantinou and Gani (1994) and Constantinou et al. (1995) used a group-contribution method to estimate T_C, P_C, and ω for a homologous series of n-alkanes. Kontogeorgis and Tassios (1997) gave a critical review of various correlations for T_C, P_C, and ω, and concluded that the group-contribution method of Constantinou and Gani (1994) and Constantinou et al. (1995) is reliable for extrapolation to extended CNs. In this research, therefore, the values from the API technical data book (Daubert and Danner, 1997) and those from the group-contribution method (Constantinou and Gani, 1994; Constantinou et al., 1995) are integrated with smooth trends. The accuracy level is kept within the experimental uncertainties for the n-alkanes for which measured values are available. Table B-1 (Appendix B) shows the resulting values for T_C, P_C, and ω for n-alkanes from C_1 through n-C_{100} that are used in this research. Equations B1 through B3 are correlations based on the tabulated values, but not used in the BIP optimization.

For type IIIa binaries, the UCEP predicted by the PR EOS shifts upward along the extension of the three-phase curve in P–T space as the BIP value is increased. This trend is reversed for type IIIb binaries. Because of this type-wise monotonic behavior of three-phase predictions, it is not difficult to find optimum BIP values by use of the exhaustive-search approach (Section S2 of Supplementary Material). With the optimized BIP for a given binary, however, the values of $\Delta T_{3\varphi}$, ΔT_{UCEP}, and ΔP_{UCEP} typically increase with increasing temperature (and pressure) along the resulting three-phase curve. This is difficult to improve since changing the only adjustable parameter, BIP, gives little control over the curvature of the three-phase curve for each binary on the basis of the PR EOS. As discussed below, therefore, not all values of $\Delta T_{3\varphi}$, ΔT_{UCEP}, and ΔP_{UCEP} can be retained within the experimental uncertainties stated by Brunner (Brunner, 1990).

Table 1 presents the optimized BIPs along with the absolute average deviations (AADs) in $T_{3\varphi}$ and the absolute deviations (ADs) in T_{UCEP} and P_{UCEP} for the 20 binaries considered. The largest AAD in $T_{3\varphi}$ is 2.99 K that occurs for the water/n-C_{11} binary. The largest AD in T_{UCEP} is 4.65 K for the water/n-C_{20} binary. These deviations of temperature predictions correspond to relative errors of lower than 1%. The AD in P_{UCEP} (i.e., ΔP_{UCEP}) is 1.34 bars for the water/n-C_{25} binary, which gives the largest ΔP_{UCEP} among the water/n-alkanes binaries with n-C_{25} and lighter. For water with n-C_{26} and heavier, the UCEP data reported are somewhat dispersed around the overall trend. When these raw data are used in Equation (3), the highest ΔP_{UCEP} of 12.70 bars occurs for the water/n-C_{28} binary.

The optimized BIP values for water with n-alkanes with CNs from 26 through 36 are constant at 0.242. This is related to the experimental fact that the three-phase curve and x_{wL} approach their asymptotic limits as the n-alkane component becomes heavier, as will be presented later in this subsection.

The optimized BIPs for water with n-alkanes are correlated with n-alkane MW by use of the following equation:

$$BIP = c_1[1 + \exp(c_2 - c_3 MW)]^{-1/c_4}, \quad (4)$$

where $c_1 = 0.24200$, $c_2 = 65.90912$, $c_3 = 0.18959$, and $c_4 = -56.81257$. The correlation gives the R^2 value of 0.9969 and the standard deviation of 0.0068 against the optimized BIPs. The maximum deviation of 0.024 occurs for 86.18 g/mol (i.e., n-C_7). The correlated values for the BIPs for the 20 binaries considered in the optimization are shown in Table 1, and also visualized in Fig. 1.

Note that only the three-phase P–T curves presented in Brunner (1990) were used in the BIP optimization. Nevertheless, the PR EOS gives reasonable accuracy for x_{wL} predictions for water/n-alkane binaries when BIPs from Equation (4) are used. Table 2 summarizes the AADs in predictions of x_{wL} for the water/n-alkane binaries for which experimentally measured x_{wL} are available. Fig. 2 presents x_{wL} predictions along the three-phase curve for the water/n-C_{20} binary, which gives the highest AAD in Table 2. The x_{wL} data were taken from Skripka (1979). The UCEP in Skripka (1979) deviates from that in Brunner (1990), based on which the BIP correlation was developed. This is why a measured x_{wL} value exists at a temperature higher than T_{UCEP} from the PR EOS in Fig. 2. The AAD for x_{wL} is 4.2 mol% with the maximum AD of 7.0 mol% for the water/n-C_{20} binary. The reasonable accuracy in the x_{wL} predictions (Table 2) is remarkable considering the simplicity of the PR EOS and the van der Waals mixing rules. Note again that the x_{wL} data have not been matched in the BIP optimization.

To see the sensitivity of phase behavior predictions through the PR EOS with Equation (4), the water/n-C_8 and water/n-C_{16} binaries are considered. The MW of n-C_8 and n-C_{16} are 114.23 and 226.44 g/mol, respectively. The results of perturbation of the n-alkane MW by 10% on the predicted UCEP are presented in Table 3. The perturbation of MW by −10% systematically increases the water/n-alkane BIP which in turn results in a longer span for the three-phase curve in P–T space. The opposite is observed for the +10% perturbation.

Fig. 3 shows three-phase P–T data for water/n-C_{16} (Brunner, 1990) and three predicted curves; one with the BIP from Equation (4), and the others with ±10% perturbations in MW with Equation (4). Fig. 3b presents the V and L phase compositions along the three-phase curves presented in Fig. 3a. These compositional predictions can be compared with the x_{wL} data measured along the three-phase curve for water/n-C_{16} (Skripka, 1979; Shaw et al., 2006b). This figure shows that x_{wL} at a given T below T_{UCEP} is predicted to be larger as the BIP becomes smaller. Matching the UCEP is necessary to give reasonable predictions of equilibrium-phase compositions along the three-phase curve.

Normal eicosane (n-C_{20}) is the heaviest n-alkane for which

Table 1
BIP values optimized in Section 2.1 and resulting deviations in three-phase curve predictions. Correlated BIP values using Equation (4) are also shown. The predicted UCEP using the optimized BIP has been rounded off to two decimal places.

CN	Lower bounds		BIP (optimized)	Number of data points	AAD in $T_{3\varphi}$	UCEP (Opt. BIP)		AD in UCEP		BIP (correlation)
	T, K	P, bars			K	T_{UCEP}, K	P_{UCEP}, bar	T_{UCEP}, K	P_{UCEP}, bar	
3	336.80	23.22	0.666	4	0.14	369.39	43.26	0.31	0.66	0.666
4	325.50	5.45	0.636	9	0.74	422.65	42.36	1.45	0.24	0.636
5	377.50	8.10	0.630	7	0.86	463.11	45.91	0.69	0.14	0.607
6	419.00	11.25	0.555	6	1.93	492.71	52.52	3.69	0.30	0.579
7	414.70	7.13	0.548	8	1.12	516.87	62.64	3.13	0.56	0.553
8	418.30	5.83	0.530	7	2.49	535.64	73.63	4.36	0.47	0.527
9	447.90	10.81	0.509	11	1.53	550.98	85.26	3.02	0.14	0.503
10	465.80	14.73	0.487	5	2.50	563.21	96.31	4.39	0.24	0.480
11	475.80	17.60	0.466	13	2.99	573.68	107.28	4.12	0.22	0.458
12	519.40	40.60	0.442	12	2.51	581.53	116.31	3.27	0.29	0.437
14	446.90	8.80	0.400	13	2.51	594.95	133.74	3.75	0.36	0.398
16	456.30	11.00	0.362	11	2.43	605.23	149.38	3.07	0.68	0.363
18	439.40	7.30	0.329	12	2.64	612.31	160.51	4.19	0.19	0.330
20	421.80	4.54	0.300	11	2.66	618.05	169.86	4.65	0.94	0.301
24	455.70	10.66	0.253	8	1.66	630.84	193.21	1.86	0.79	0.250
25	451.40	9.70	0.243	15	2.47	636.29	203.54	0.11	1.34	0.243
28	533.80	47.50	0.242	10	1.14	649.59	227.10	8.39	12.70	0.242
30	502.50	27.60	0.242	13	0.64	647.49	221.80	5.89	8.30	0.242
32	499.30	26.12	0.242	10	1.02	647.07	220.68	4.97	8.68	0.242
36	549.30	60.90	0.242	8	0.92	647.06	220.60	4.66	5.70	0.242

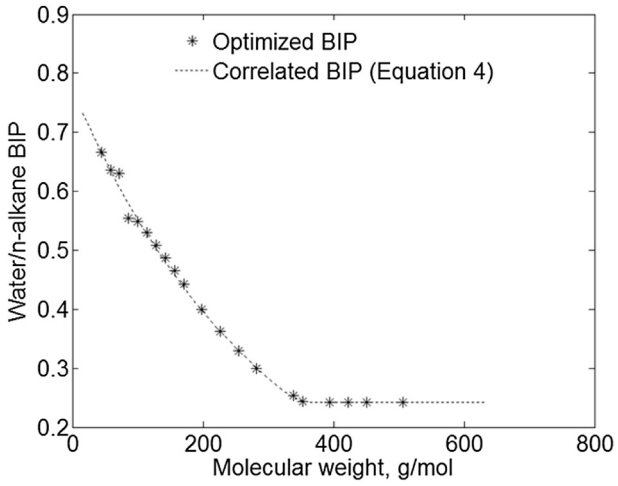

Fig. 1. Correlation of the optimized BIPs for water/n-alkane binaries based on three-phase P–T curves measured by Brunner (1990).

measured x_{wL} data were reported in the literature. Normal hexatriacontane (n-C_{36}) is the heaviest n-alkane measured in Brunner (1990). Fig. 4 presents the asymptotic behavior of x_{wL} predictions for water with four n-alkanes, n-C_8, n-C_{20}, n-C_{32}, and n-C_{100}. The sensitivity of x_{wL} at a fixed temperature (e.g., 450 K, or 1/T = 2.2 × 10^{-3}) to n-alkane CN tends to diminish as the n-alkane component becomes heavier as long as temperature is not close to the corresponding T_{UCEP}. The behavior of x_{wL} near T_{UCEP} for type IIIa is different from that for type IIIb. The former exhibits a somewhat convex shape in Fig. 4 since the L phase should merge with the V phase, not with the W phase, at the UCEP. This is not the case for type IIIb. Use of Equation (4) yields a constant BIP of 0.242 for water with n-alkanes heavier than n-C_{25}. If the BIP values are not kept constant for water with heavier n-alkanes, the asymptotic behavior of x_{wL} cannot be predicted due to the effect of BIP on x_{wL} as will be discussed in Section 2.2.

Further investigation is made into the application of Equation (4) for water with C_1 and C_2. Equation (4) gives 0.732 for water with C_1 and 0.696 for water with C_2, while Peng and Robinson (1976b) recommended 0.500 for both binaries. They obtained these values using the experimental measurements of Olds et al. (1942) and Reamer et al. (1943) for the two binaries.

Olds et al. (1942) and Reamer et al. (1943) measured the V-phase composition in equilibrium with the W phase for the water/C_1 and water/C_2 binaries, respectively. Measurements were made for pressures up to 689.48 bars at seven different temperatures 310.93 K, 344.26 K, 377.59 K, 410.93 K, 444.26 K, 477.59 K, and 510.93 K. Only pressures lower than the critical point of water (220.64 bars) are considered for the evaluation because the intended application of Equation (4) is in the simulation of thermal recovery processes. Thus, the highest pertinent value for the system pressure used in this assessment is 206.84 bars. The evaluation for

Table 2
Deviations of predicted water solubilities in the L phase (x_{wL}) for a few different water/n-alkane binaries.

CN	Number of data points	AAD in x_{wL}	Data sources	Average uncertainty in x_{wL} data
3	9	0.003	Kobayashi and Katz (1953)	0.001
4	7	0.003	Reamer et al. (1944)	0.005
6	6	0.022	Skripka (1979), Tsonopoulos and Wilson (1983), Maczynski et al. (2005)	0.027
7	4	0.008	Skripka (1979)	0.055
8	5	0.018	Skripka (1979), Heidman et al. (1985), Shaw et al. (2005)	0.066
9	5	0.026	Skripka (1979)	0.098
10	6	0.009	Skripka (1979), Shaw et al. (2006a)	0.101
12	3	0.022	Skripka (1979)	0.139
16	5	0.022	Skripka (1979), Shaw et al. (2006b)	0.113
20	6	0.042	Skripka (1979)	0.170

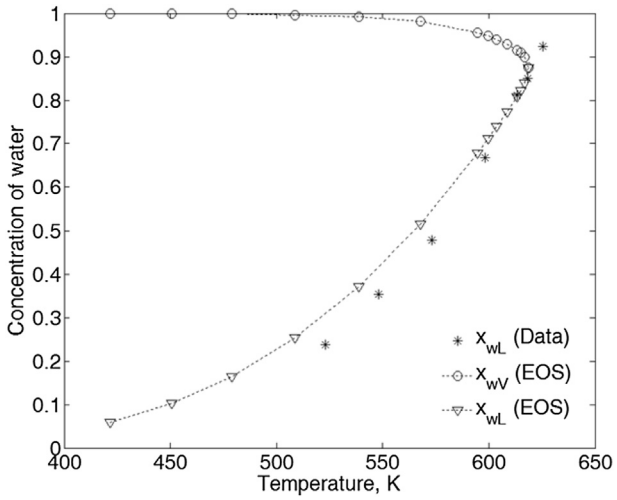

Fig. 2. Non-aqueous phase compositions predicted by the PR EOS with the BIP correlation (Equation (4)), and solubilities of water in the L phase (x_{wL}) measured along the three-phase curve of water/n-C_{20} system (Skripka, 1979).

Table 3
Sensitivity of predicted UCEP for water/n-C_8 and water/n-C_{16} binaries using the PR EOS with Equation (4) to perturbation in n-alkane MW. Δ stands for the perturbation. Negative perturbations of the n-alkane MW result in higher values for the BIP. This in turn results in a longer span of the three-phase curve calculated in P–T space. The opposite is observed for the positive perturbations.

CN	Δ	MW, g/mol	BIP (Eqn. (4))	P_{UCEP}, bars	T_{UCEP}, K
8	0%	114.23	0.527	73.42	535.43
8	10%	125.65	0.508	72.04	534.10
8	−10%	102.81	0.548	75.00	536.97
16	0%	226.44	0.363	150.01	605.57
16	10%	249.09	0.336	136.57	598.23
16	−10%	203.80	0.391	173.71	617.88

the water/C_1 and water/C_2 binaries considers 65 and 66 data points, respectively.

The AADs for the predicted x_{wV} with Equation (4) are 0.0064 for water/C_1 and 0.0086 for water/C_2. For both binaries, the maximum deviation in x_{wV} (0.0329 for water/C_1, 0.0488 for water/C_2) occurs at 510.93 K and 206.84 bars. Olds et al. (1942) stated that the uncertainty associated with their composition measurements is about 2%. Over the considered set of 65 points, the average uncertainty in x_{wV} measurements is approximately 0.0023. Reamer et al. (1943) did not specify uncertainty values for their composition measurements. The BIP values recommended by Peng and Robinson (1976b) result in similar AADs for the same set of data; 0.0013 for water/C_1 and 0.0032 for water/C_2. Given these results, it is reasonable to conclude that Equation (4) can be extrapolated for BIPs for water with C_1 and C_2.

2.2. Comparison of the new BIPs with other recommended values

In this subsection, the significance of Equation (4) is elucidated by comparing predictions made using it with those made with a BIP value of 0.5, which is a representative value from the literature (Heidman et al., 1985; Peng and Robinson, 1976b; Tsonopoulos and Heidman, 1986; Nasrifar and Moshfeghian, 2002; Eubank et al., 1994; Mohebbinia et al., 2013; Søreide and Whitson, 1992). Equation (4) gives a much lower value of 0.242 for water with heavy n-alkanes (see Table 1). A review of prior investigations pertaining to the optimal values for the BIP for water with n-alkanes is presented in Section S1 of Supplementary Material.

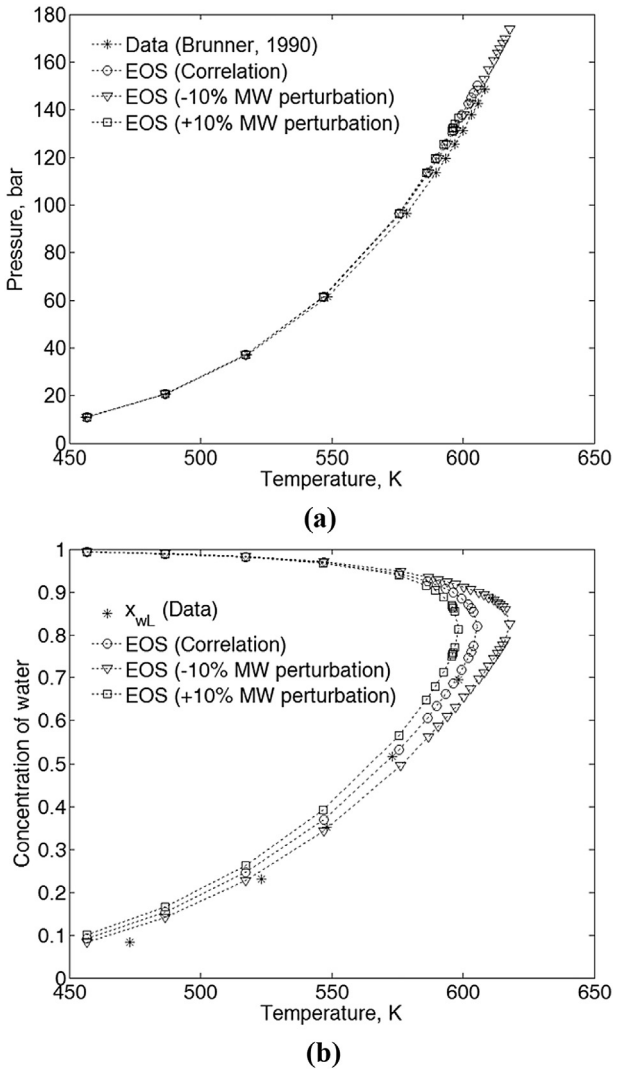

Fig. 3. Effect of molecular-weight (MW) perturbation in Equation (4). (a) Effect on the three-phase curve predicted for the water/n-C_{16} binary. (b) Effect on the V- and L-phase compositions predicted along the three-phase curve for the water/n-C_{16} binary. The L-phase composition data were taken from Skripka (1979) and Shaw et al. (2006b).

Fig. 5 shows the dimensionless molar Gibbs free energy change on mixing ($\Delta_m G/RT$) at 100.00 bars and 571.88 K ($T_r = 0.98$) for water with n-C_{12}. The BIP value 0.437 from Equation (4) is used in Fig. 5a, and 0.500 is used in Fig. 5b. In Fig. 5a, the three equilibrium phases are shown as tangent points on the Gibbs free energy. The x_{wL} and x_{wV} are 0.5469 and 0.8259, respectively. The W phase consists of nearly 100% water. As the BIP is increased from 0.437 to 0.500 at the same pressure and temperature, the Gibbs free energy systematically shifts upward, resulting in the W–L equilibrium. The right lobe of the Gibbs free energy associated with the L phase keeps the level of convexity as it is displaced upward. Then, the x_{wL} ($=1.0 - x_{hcL}$) becomes lower as the BIP is increased since the tangent slope from the W phase onto the L-phase lobe becomes greater. With the BIP of 0.500, temperature must be increased to 573.08 K to predict the three-phase equilibrium at 100.00 bars. The resulting x_{wL} and x_{wV} are 0.4602 and 0.8567, respectively.

The effect of the BIP value on prediction of the three-phase curve is shown in Fig. 6 for the water/n-C_{12} binary. As the BIP is increased, the UCEP is extended to higher pressure and temperature. The PR EOS with the BIP value of 0.500 erroneously predicts

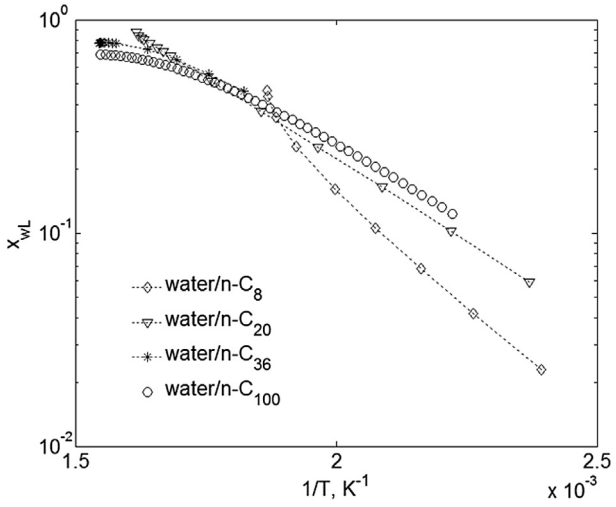

Fig. 4. Trends in x_{wL} predicted along the three-phase curves for the water binaries with n-C_8, n-C_{20}, n-C_{36}, and n-C_{100}. The horizontal axis ranges from 400 ($1/2.5 \times 10^3$) K to 667 ($1/1.5 \times 10^3$) K.

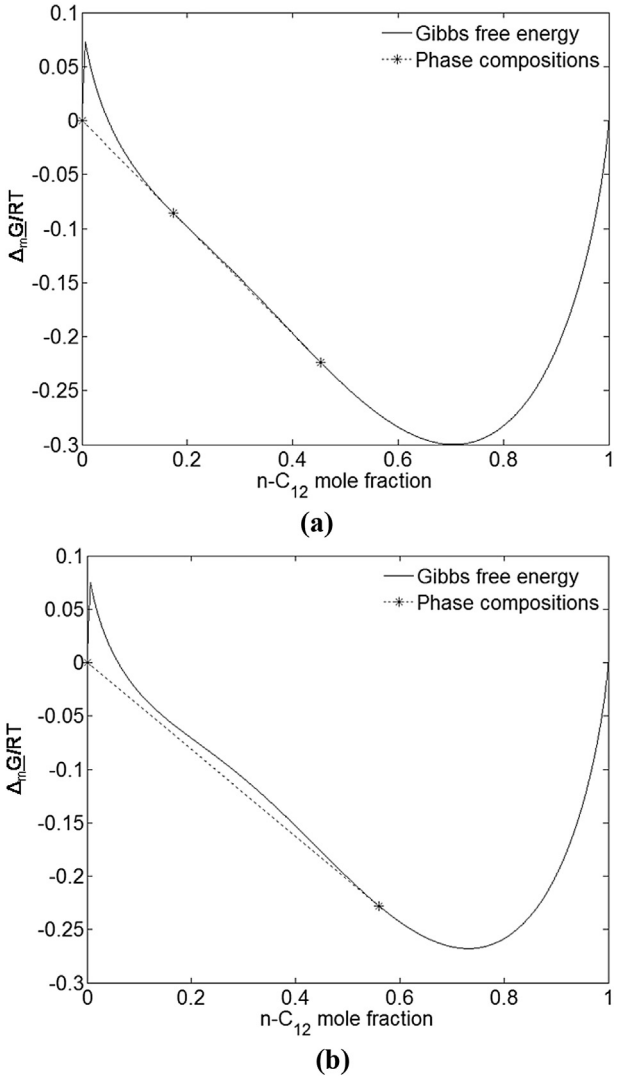

Fig. 5. Dimensionless molar Gibbs free energy change on mixing predicted by the PR EOS for the water/n-C_{12} binary at 100.00 bars and 571.88 K; (a) BIP = 0.437 and (b) BIP = 0.500. In (a), the three equilibrium phases are presented by the tangent points. The BIP (0.437) used was obtained from Equation (4). In (b), the two equilibrium phases are presented by the tangent points. The BIP used is 0.500. As the BIP is increased from 0.437 to 0.500 at the same pressure and temperature, the Gibbs free energy systematically shifts upward, resulting in the W-L equilibrium. With the BIP of 0.500, temperature must be increased to 573.08 K to predict the three-phase equilibrium at 100.00 bars.

the UCEP for water with n-C_{12} at 135.43 bars and 593.55 K. Accurate prediction of the UCEP is important since it is the limiting three-phase behavior. Fig. 6b compares the x_{wL} and x_{wV} along the three-phase curves by use of the BIP value 0.437 from Equation (4) and 0.500. The W phase consists of nearly 100% water, and is not shown in Fig. 6b. It clearly shows how the overprediction of the UCEP results in underprediction of x_{wL} and overprediction of x_{wV}.

The effect of the BIP on the three-phase curve becomes much less as the n-alkane component becomes heavier. This is especially true for binaries of type IIIb (e.g. water with n-C_{30}). The less sensitivity is likely because the W and V phases merge at the UCEP very close to 100% water in composition space, where the BIP little affects phase behavior predictions. However, the L-phase composition (i.e., x_{wL}) is still affected significantly by the BIP value used because it is well inside composition space. Fig. 7 compares phase compositions along the three-phase curve for water with n-C_{30} with two BIP values; 0.242 from Equation (4) and 0.500. Although the UCEP temperatures are quite similar, the x_{wL} predictions are substantially different from each other.

The PR EOS with BIPs for water with n-alkanes from Equation (4) predicts type IIIa up to n-C_{25} and type IIIb for n-C_{26} and heavier. In Brunner (1990), type IIIa was observed for water/n-alkane binaries up to n-C_{25}, and type IIIb for water/n-C_{28} and heavier. Fig. 8 shows that type IIIa is predicted for the water/n-C_{25} binary with the BIP value 0.243 from Equation (4), but type IIIb is erroneously predicted with the BIP value of 0.500. Since the critical point between the V and L phases in Fig. 8a occurs near the coexisting W phase, the V phase merges with the W phase at the UCEP for water with the next n-alkane n-C_{26}. The BIP of 0.500 results in significantly lower x_{wL} than the value from Equation (4), indicating the importance of accurate representation of three-phase behavior.

2.3. Validation of the BIP correlation for water with multicomponent n-alkane mixtures

This subsection is concerned with the accuracy of the PR EOS when it is used with the BIP correlation (Equation (4)) for water with multicomponent n-alkane mixtures. The validation of Equation (4) against the measured data for multicomponent water/n-alkane mixtures is necessary as these data were not considered in the development of Equation (4). The BIPs between hydrocarbon components are set to zero for all case studies.

McKetta and Katz (1948) gave tie triangles measured for the water/C_1/n-C_4 ternary at different P–T conditions. Fig. 9 compares the prediction with the data at 377.6 K and 44.88 bars. The V-phase composition exhibits the highest deviation, but the difference is only 6.73 mol% in the C_1 concentration. Although not shown in this paper, similar agreements in terms of three equilibrium-phase compositions were obtained at two other P–T conditions reported (85.56 and 58.95 bars at 377.6 K).

The distance in composition space between the measured and predicted compositions is calculated as $\delta_j = \left\| \underline{x}_j^{EOS} - \underline{x}_j^{Data} \right\|_2$ for phase j, where $\underline{x}_j$ is the vector consisting concentrations of the three components. The BIPs of Peng and Robinson (1976b) yield 0.100, 1.18×10^{-2}, and 8.94×10^{-4} for δ_V, δ_L, and δ_W, respectively. The BIPs from Equation (4) yield 0.100, 9.64×10^{-3}, and 8.99×10^{-4} for δ_V,

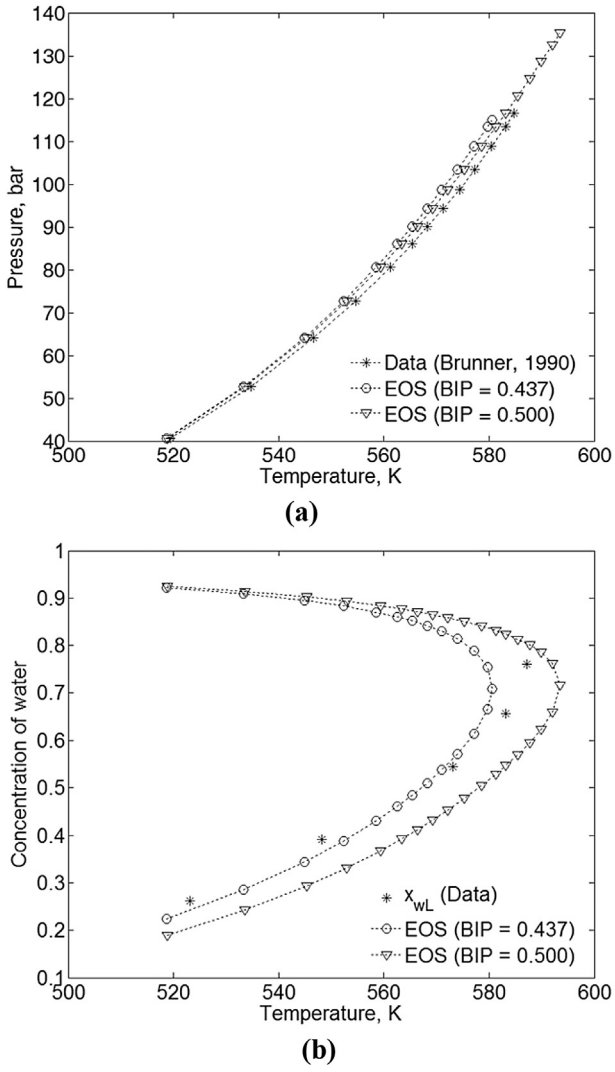

Fig. 6. Effect of BIP on phase behavior predictions for the water/n-C_{12} binary. (a) Effect on the three-phase curve prediction. (b) Effect on the compositions of the V and L phases along the three-phase curve. The data for the L-phase composition was taken from Skripka (1979). Application of the commonly used BIP value of 0.500 to predict the three-phase curve of type IIIa binaries can result in the overestimation of its span in P–T space. The mechanism for this is a systematic overestimation of x_{wV} and underestimation of x_{wL}.

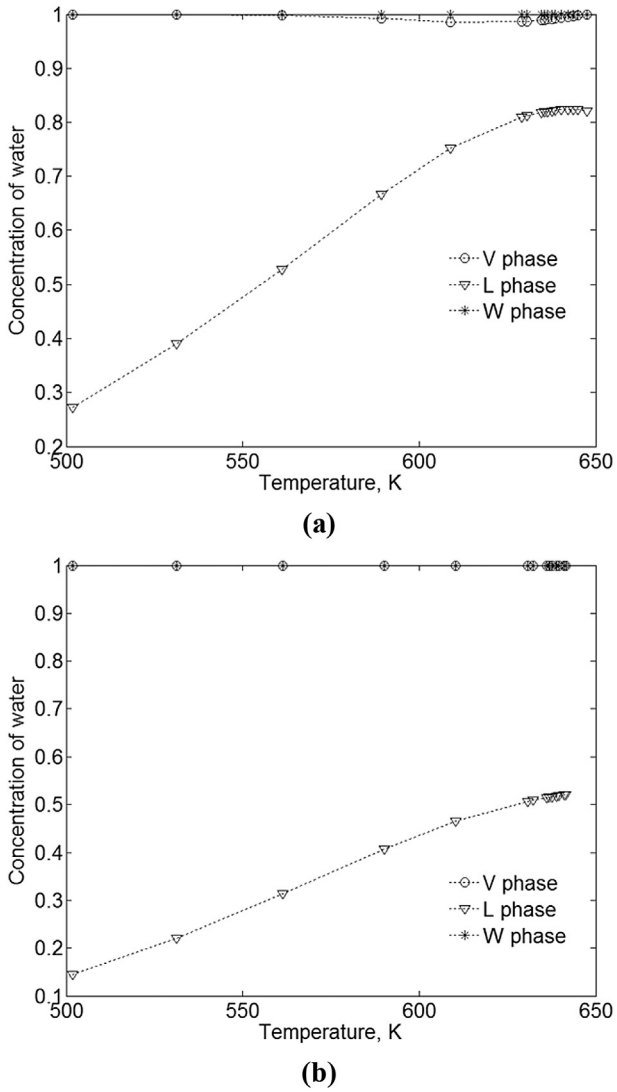

Fig. 7. Phase compositions predicted by the PR EOS along the three-phase curve of the water/n-C_{30} binary; (a) BIP = 0.242 (on the basis of Equation (4)) and (b) BIP = 0.500. Note the change in the predicted compositions for the V and L phases in (b) in comparison with (a). The predicted solubilities of water in the L phase are substantially lower than when the BIP from Equation (4), 0.242, is used. Measurements for the phase compositions for this system at these conditions have not been published in the literature.

δ_L, and δ_W, respectively.

Chawla et al. (1995) reported experimental data for the V-phase composition for the water/n-C_{10}/n-C_{15} ternary at 533.15 K and 52.44 bars. With a composition distance of 0.0363, the predicted V-phase composition is close to that measured. The L phase contains 29.27 mol% of water at these P–T conditions, indicating the potential importance of considering x_{wL} in reservoir studies.

Barrufet et al. (1996) presented measured compositions of the V, L, and W phases for a quaternary mixture of 75.97% water, 12.92% C_3, 5.44% n-C_5, and 5.67% n-C_8 at six different P–T conditions. Table 4 summarizes the comparison between the data and predictions from the PR EOS with BIPs from Equation (4). The deviations from the data are expressed using the composition distance δ_j for phase j as previously defined. The values for δ_L for all cases are lower than 0.1 indicating that the predicted values for the L-phase are reasonably close to the data. The largest deviations from the data were observed at 448 K and 51.50 bars. The corresponding values for δ_L and δ_V at these conditions are 0.0916 and 0.1278, respectively.

Chawla et al. (1995) presented the V-phase compositions of three-phase equilibria measured for three different quaternary systems at different P–T conditions. Their approximate compositions were 69% water, 10% n-C_6, 10% n-C_7, and 11% n-C_8; 76% water, 12% n-C_7, 7% n-C_9, and 5% n-C_{12}; and 98% water, 0.2% n-C_{10}, 0.8% n-C_{15}, and 1% n-C_{20}. Table 5 gives comparisons between the data and predictions for these cases. In Table 5, the aforementioned systems have been labeled as systems 1, 2 and 3, respectively. Water has been assigned an index of 1. The n-alkanes have been assigned indices 2, 3 and 4 in the order of increasing CN. The largest value for δ_V (0.2436) occurs for water/n-C_6/n-C_7/n-C_8 system at 438.71 K and 12.94 bars. The values for δ_V presented in Table 5 indicate that Equation (4) can yield reasonably accurate predictions for the V-phase composition for multicomponent systems over a wide range of temperatures, pressures, and CNs.

The highest x_{wL} value calculated in these cases is 0.3336 for the

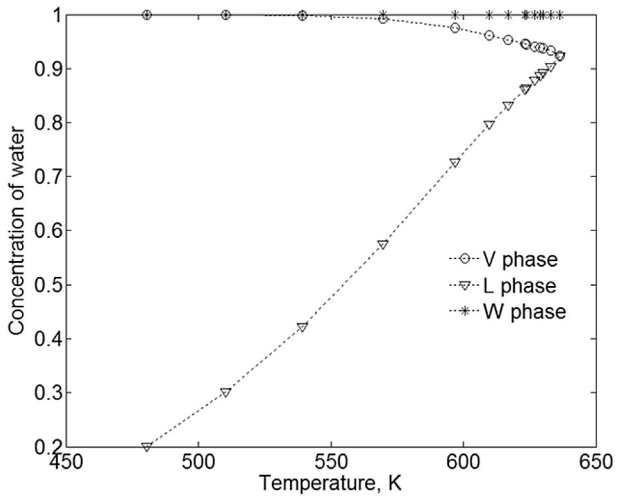

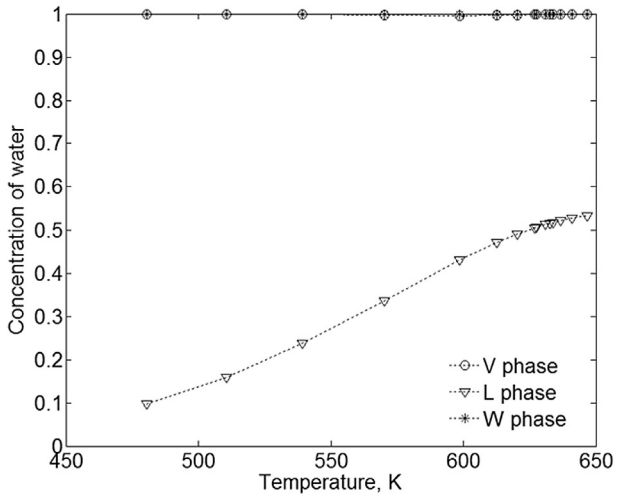

Fig. 8. Phase compositions predicted by the PR EOS along the three-phase curve of the water/n-C_{25} binary; (a) BIP = 0.243 from Equation (4) yields type IIIa phase behavior, where the V and L phases merge at the UCEP. This is consistent with the experimental results of Brunner (1990). (b) BIP = 0.5 results in type IIIb phase behavior, where the V and W phases merge at the UCEP. This is inconsistent with the experimental results of Brunner (1990). Measurements for the phase compositions for this system at these conditions have not been published in the literature.

water/n-C_{10}/n-C_{15}/n-C_{20} system at 533.15 K and 49.00 bars. Although there are no experimental data to compare, this value is plausible considering that even higher x_{wL} values have been reported for water-containing oil mixtures at similar temperatures, as discussed in the next subsection.

2.4. Application of the BIP correlation for characterization of water-containing reservoir oil

Results presented in Griswold and Kasch (1942), Tsonopoulos and Wilson (1983), and Heidman et al. (1985) show that x_{wL} becomes higher with increasing level of aromaticity in the L phase. This is consistent with the discussion of Tsonopoulos and Wilson (1983) that the affinity towards water is lowest for n-alkanes and highest for aromatics. Since reservoir oils contain a variety of hydrocarbon compounds, such as paraffins, naphthenes, and aromatics, the PR EOS with the BIP correlation developed for n-alkanes

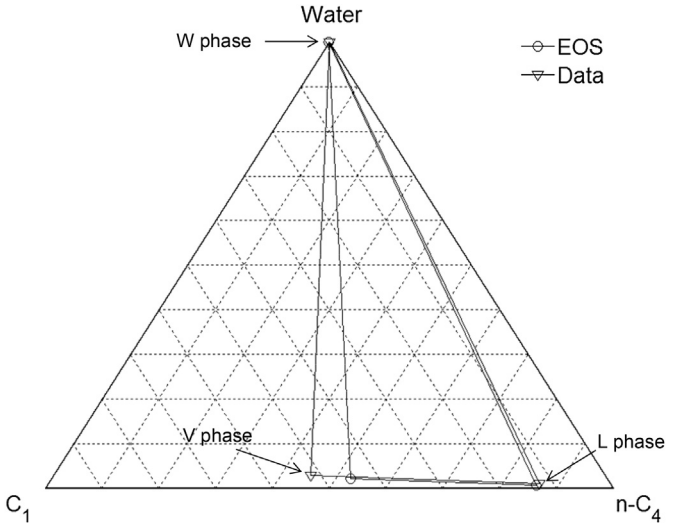

Fig. 9. Tie triangle predicted by the PR EOS with the BIP correlation (Equation (4)) for the water/C_1/n-C_4 system at 377.60 K and 44.88 bars. The phase compositions measured by McKetta and Katz (1948) are also shown.

Table 4
Deviations of predicted three-phase compositions for a mixture of 75.97% water, 12.92% C_3, 5.44% n-C_5, and 5.67% n-C_8. The deviations are expressed as distances (δ) in composition space. The definition of δ is presented in Section 2.3.

Case	T, K	P, bar	δ_V	δ_L	δ_W
1	313.00	7.00	0.01140	0.02102	0.00087
2	338.00	11.76	0.01768	0.03595	0.00003
3	373.00	20.34	0.08276	0.03395	0.00027
4	393.00	26.33	0.09204	0.03330	0.00032
5	423.00	39.30	0.07134	0.05695	0.00130
6	448.00	51.50	0.12779	0.09156	0.00318

(Equation (4)) is expected to yield systematic underpredictions of x_{wL} for water-containing reservoir oils.

An Athabasca bitumen has been characterized by use of the method of Kumar and Okuno (2013, 2014) along with experimental data presented in Badamchi-Zadeh et al. (2009a, 2009b). Properties used in the PR EOS model for the water/Athabasca-bitumen mixture are presented in Table 6. Flash calculations have been performed at the experimental P–T conditions given in Amani et al. (2013a, 2013b). Table 7 shows that the predicted x_{wL} values are systematically lower than the measured values at the conditions considered in Amani et al. (2013a, 2013b). This is expected since the BIP correlation used has been developed for water with n-alkanes. The predicted x_{wL} monotonically increases with increasing temperature, which is in line with the reported data.

Similar calculations are conducted for the Peace River bitumen. The experimental data presented in Mehrotra and Svrcek (1985) are used for characterization of the bitumen. Table 8 shows properties used in the fluid model for the water/Peace-River-bitumen mixture. In Table 9, predictions are compared with the x_{wL} data presented in Glandt and Chapman (1995). Glandt and Chapman (1995) presented temperatures for the x_{wL} data points reported, but not the corresponding pressures. It is reasonable to assume that their measurements were made at pressures on the boundary between two and three phases so that the W phase could exist (Chapman 2014[1]). The predicted results given in Table 9 are based

[1] Personal communication with Professor W.G. Chapman, Rice University, Houston, Texas.

Table 5
Deviations of predicted V-phase compositions for quaternary mixtures presented in Chawla et al. (1995). Systems 1, 2 and 3 are mixtures of water/n-C_6/n-C_7/n-C_8, water/n-C_7/n-C_9/n-C_{12}, water/n-C_{10}/n-C_{15}/n-C_{20}, respectively. The respective overall compositions at which the measurements were made are specified in Section 2.3. Water has been assigned an index of 1. The n-alkanes have been assigned indices 2, 3 and 4 in the order of increasing CN.

System number	T	P	x_{iV} (EOS)				x_{iV} (data)				δ_V
	K	bar	i = 1	i = 2	i = 3	i = 4	i = 1	i = 2	i = 3	i = 4	
1	399.82	4.53	0.5178	0.1987	0.1618	0.1217	0.4800	0.2700	0.1500	0.1000	0.0844
1	416.48	6.87	0.5589	0.1484	0.1475	0.1452	0.4900	0.2500	0.1700	0.0900	0.1365
1	438.71	12.94	0.5280	0.2184	0.1504	0.1032	0.3200	0.3000	0.2400	0.1400	0.2436
1	455.37	19.00	0.5300	0.2181	0.1484	0.1035	0.5700	0.1800	0.1400	0.1100	0.0562
1	472.04	26.80	0.5346	0.2001	0.1504	0.1149	0.4500	0.2300	0.1700	0.1500	0.0983
1	488.71	36.59	0.5380	0.1682	0.1534	0.1404	0.6500	0.1300	0.1000	0.1200	0.1314
1	510.93	52.86	0.5566	0.1406	0.1465	0.1563	0.6000	0.1300	0.1300	0.1400	0.0503
2	404.82	3.50	0.7939	0.1349	0.0587	0.0125	0.8000	0.1500	0.0480	0.0020	0.0221
2	416.48	5.70	0.6821	0.2610	0.0504	0.0065	0.7500	0.1750	0.0600	0.0150	0.1103
2	438.71	10.00	0.7026	0.2337	0.0549	0.0089	0.7800	0.1500	0.0650	0.0050	0.1145
2	455.37	14.90	0.7020	0.2311	0.0563	0.0105	0.7300	0.1800	0.0700	0.0200	0.0606
2	472.04	21.30	0.7085	0.2172	0.0608	0.0135	0.7700	0.1400	0.0600	0.0300	0.1001
2	488.71	29.90	0.7058	0.2115	0.0655	0.0172	0.7500	0.1500	0.0800	0.0200	0.0772
2	510.93	42.93	0.7473	0.1453	0.0735	0.0339	0.7000	0.1700	0.1200	0.0100	0.0747
2	527.59	56.24	0.7565	0.1188	0.0735	0.0511	0.7700	0.1100	0.0800	0.0400	0.0206
3	394.26	2.00	0.9971	0.0014	0.0014	0.0001	0.9600	0.0300	0.0009	0.0091	0.0477
3	422.04	4.50	0.9962	0.0015	0.0022	0.0002	0.9450	0.0500	0.0010	0.0040	0.0706
3	449.82	9.40	0.9872	0.0086	0.0037	0.0004	0.9450	0.0540	0.0009	0.0001	0.0621
3	477.59	17.40	0.9872	0.0063	0.0055	0.0010	0.9400	0.0580	0.0019	0.0001	0.0701
3	505.37	30.00	0.9840	0.0058	0.0080	0.0022	0.9350	0.0590	0.0030	0.0030	0.0725
3	533.15	49.00	0.9755	0.0079	0.0120	0.0046	0.9350	0.0590	0.0030	0.0030	0.0658

Table 6
Properties of the Athabasca bitumen containing water. BIPs with water are based on Equation (4). Data given in Badamchi-Zadeh et al. (2009a, 2009b) were used to characterize PC1, PC2, PC3, and PC4.

Component	z_i	MW, g/mol	T_C, K	P_C, bar	ω	BIP with water
Water	0.8115	18.01	647.10	220.64	0.3433	0.000
PC1	0.0754	345.52	1024.88	17.54	0.8503	0.246
PC2	0.0493	528.46	1137.29	13.35	1.0564	0.242
PC3	0.0376	692.98	1207.42	11.20	1.1782	0.242
PC4	0.0262	996.26	1292.51	8.78	1.3301	0.242

Table 7
Water solubilities predicted near the V–L–W/L–W boundary for the water/Athabasca-bitumen mixture given in Table 6. Experimental data were taken from Amani et al. (2013a,b). The water concentrations for the V and W phases were predicted to be greater than 0.999. A stable single phase is indicated by "–". The factor, λ, is a scaling factor used to extend Equation (4) to represent x_{wL} data measured for water-containing reservoir oil. For water/Athabasca-bitumen, the value of 0.415 gives reasonably accurate estimates for x_{wL}.

P, bar	T, K	x_{wL} (data)	x_{wL} (EOS, λ = 1)	x_{wL} (EOS, λ = 0.415)
60.42	548.20	0.5412	0.3402	0.5446
87.18	573.10	0.6321	0.4116	0.6386
100.25	583.20	0.6699	0.4406	0.6770
114.50	593.10	0.7192	0.4687	0.7157
131.00	603.50	0.7477	0.4969	0.7546
148.30	613.40	0.7964	0.5222	0.7924
167.20	623.20	0.8274	0.5451	–
189.90	633.80	0.8462	0.5670	–
216.47	644.00	0.8620	0.5854	–

Table 8
Properties of the Peace River bitumen containing water. BIPs with water are based on Equation (4). Data given in Mehrotra and Svrcek (1985) were used to characterize PC1, PC2, PC3, and PC4.

Component	z_i	MW, g/mol	T_C, K	P_C, bar	ω	BIP with water
Water	0.7300	18.01	647.10	220.64	0.3433	0.000
PC1	0.0961	330.22	773.64	15.08	0.7907	0.257
PC2	0.0650	505.04	836.99	11.48	0.9932	0.242
PC3	0.0485	662.27	870.20	9.57	1.1151	0.242
PC4	0.0604	952.11	902.17	7.41	1.2654	0.242

Table 9
Water solubilities predicted near the V–L–W/L–W boundary for the water/Peace-River-bitumen mixture given in Table 8. Experimental data were taken from Glandt and Chapman (1995). The water concentrations for the V and W phases were predicted to be greater than 0.99.

P, bar	T, K	x_{wL} (data)	x_{wL} (EOS, λ = 1)	x_{wL} (EOS, λ = 0.78)
9.94	452.65	0.1800	0.1235	0.1497
15.35	472.15	0.2800	0.1670	0.1993
24.41	495.15	0.3200	0.2302	0.2703
33.43	512.15	0.3600	0.2854	0.3315
46.74	531.65	0.3700	0.3577	0.4110
69.94	557.15	0.5300	0.4663	0.5299

on this assumption. As expected, the x_{wL} predictions with the BIP correlation are systematically lower than the measured values.

As presented in Subsection 2.1, the x_{wL} predicted by the PR EOS tends to increase with decreasing BIP at a given three-phase temperature for a given binary. Therefore, the method proposed in this paper is to systematically reduce BIPs from the values given by Equation (4) for more accurate representation of x_{wL} for water-containing reservoir oils. Hence, the BIPs presented in Tables 6 and 8 are systematically reduced by the λ factor, which is 0.415 for the water/Athabasca-bitumen system and 0.780 for the water/Peace-River-bitumen system. Tables 7 and 9 present that the resulting x_{wL} predictions are closer to the measured values than those based on the water/n-alkane BIPs.

To the best of our knowledge, water/Athabasca-bitumen and water/Peace-River-bitumen are the only water-containing bitumens for which x_{wL} data have been published. Glandt and Chapman (1995) published x_{wL} measurements for three other water-containing oils, Coalinga, Huntington Beach, and Cat Canyon. However, the unavailability of data to properly characterize these oils into pseudo components restricted the extension of Equation (4) for these oils. Nevertheless, x_{wL} measurements for these oils were used to validate Equation (4) by first characterizing these oils into a homologous series of n-alkanes based on the CN distributions given in Glandt and Chapman (1995), and subsequently comparing the predicted and measured x_{wL} values. As expected, the n-alkane assumptions (both in pseudo components' properties and BIPs for

water with pseudo components) resulted in underestimations of x_{wL}, although this validation is only qualitative in the absence of comprehensive data.

The primary purpose of the development of the BIP correlation (Equation (4)) was the quantitative prediction of x_{wL} for water with n-alkanes. The solubilities of hydrocarbons in the W phase (x_{hcW}) are orders of magnitude lower than x_{wL} (Heidemann, 1974). They may be negligible for most reservoir engineering applications even at elevated temperatures (Luo and Barrufet, 2005). For example, x_{hcW} for the water/n-C_8 binary are lower than 0.01 mol% at 500 K (Heidman et al., 1985). The x_{hcW} becomes even smaller as the n-alkane becomes heavier (Luo and Barrufet, 2005). Thermodynamic modeling of x_{hcW} was studied using EOSs with elaborate mixing rules (Heidman et al., 1985; Economou et al., 1997; Søreide and Whitson, 1992; Huron and Vidal, 1979; Aparicio-Martínez and Hall, 2007). Henry's law, however, has been also satisfactorily used for representing x_{hcW} (Tsonopoulos and Wilson, 1983; Heidman et al., 1985; Economou et al., 1997; Mehra et al., 1982; Li and Nghiem, 1986). When the PR EOS is used with the BIP correlation (Equation (4)), x_{hcW} is calculated to be orders of magnitude lower than the data presented in the literature. Hence, Equation (4) is not recommended for applications in which quantitative predictions of x_{hcW} are important. It is a known limitation that a single cubic EOS with the van der Waals mixing rules cannot model x_{wL} and x_{hcW} simultaneously over a wide temperature range (Nasrifar and Moshfeghian, 2002; Heidemann, 1974; Daridon et al., 1993; Satyro et al., 2013). Furthermore, the W-phase density is underestimated with the PR EOS, but can be corrected by volume shift, or simply by using the saturated liquid density of water at the temperature of interest.

3. SAGD simulation case study

As presented in the preceding section, x_{wL} tends to increase with increasing temperature and aromaticity in the L phase. Hence, the effect of x_{wL} is expected to be pronounced in steam-based thermal recovery of bitumen. However, how much it affects bitumen recovery is uncertain in the literature. This section presents a simulation case study for SAGD, which is the most widely used method for in-situ bitumen recovery.

Reservoir flow simulations are performed using the STARS simulator of Computer Modeling Group (2011). The phase behavior predicted using the PR EOS is reflected in the simulations in terms of component K values, defined as the ratio of concentration in one phase to another, tabulated as functions of temperature and pressure.

Only a half of SAGD steam chamber is simulated for a simple homogeneous reservoir model. The properties of the reservoir model used in this simple case study have been obtained from Keshavarz et al. (2014a). The dimensions of the reservoir model used are 70.0 m × 37.5 m × 20.0 m in the x, y and z directions, respectively. The model is discretized into 70 × 1 × 20 grid blocks in the x, y and z directions, respectively, for finite-difference simulations with STARS. The reservoir is situated at a depth of 500 m. The production well is located 3 m above the bottom of the reservoir model, and the injection well is located 4 m above the production well. Both wells are situated in the first grid block immediately adjacent to the left edge of the reservoir model.

The operating pressure is 40 bars. Steam of 90% quality is injected at the saturation temperature (approximately 524 K) at 40 bars. The initial reservoir temperature is 286.15 K. The maximum bottomhole pressure (BHP) for the injection well is set to 40 bars. The production well is subject to a minimum BHP of 15 bars, which is the initial reservoir pressure, and a maximum steam flow rate of 1 m^3/day. The reservoir is subject to an initial heating period of 6 months using steam. The initial saturation of water in the reservoir is 0.25, with the remainder being live bitumen. The residual saturation of oil is assumed to be 0.13. The relative permeability model used is independent of temperature. Other effects such as dispersion, capillarity and asphaltene precipitation are not considered. The pertinent information of this reservoir model is summarized in Table 10.

The live bitumen used in the simulations is a mixture of 4 mol% methane (C_1) and 96 mol% dead Athabasca bitumen (C_D). This corresponds to a gas-to-oil-ratio (GOR) of 1.8 m^3/m^3. The properties of C_D are taken from Mehrotra and Svrcek (1986, 1987); the T_C, P_C and ω of C_D are 1090.90 K, 7.86 bars, and 1.3611, respectively. The molecular weight of C_D is 594.60 g/mol, and its specific gravity at the initial reservoir temperature is 1.077. The bitumen comprises 19.2 wt% asphaltenes, 39.8 wt% distillable maltenes and 41.2 wt% undistillable maltenes (Mehrotra and Svrcek, 1987).

The SAGD simulations in this section use three components, water, C_1, and C_D. The pertinent BIPs are 0.732 for C_1 with water, 0.100 for C_D with water, 0.1174 for C_1 with C_D (Keshavarz et al., 2014a). Two fluid models are considered to ascertain the effect of x_{wL} on bitumen recovery in SAGD, which are referred to as the base and modified cases. The base case corresponds to current practice of SAGD simulation with the assumption of no water dissolution in the L phase even at operating temperatures, which can be higher than 500 K. The modified case properly considers x_{wL} by using the systematic adjustment of BIPs presented in Section 2 along with x_{wL} data measured for an Athabasca bitumen (Amani et al., 2013a, 2013b). Both cases assume that the W phase consists of 100% water (i.e., x_{hcW} is zero).

For the base case, the hydrocarbon part (C_1 and C_D) is modeled by K values based on the L–V equilibrium predicted from the PR EOS. The water K values for the V–W equilibrium are generated by use of Raoult's law, as conventionally done in the literature (Keshavarz et al., 2014a, 2014b, 2015).

For the modified case, the entire ternary phase behavior is represented by K values for the L, V, and W phases predicted by the PR EOS with water, C_1, and C_D. The K values in the STARS simulator are dependent on pressure and temperature, but independent of composition. Therefore, an overall composition of 90 mol% water, 0.4 mol% C_1, and 9.6 mol% C_D is specified for providing K values for the simulator. This overall composition corresponds to 90 mol% water and 10 mol% live bitumen, and is representative of mixtures near the steam-chamber edge. Winprop of (Computer Modeling Group 2011) was used to perform the necessary flash calculations to compute the K values.

Liquid-phase densities and viscosities in the STARS simulator are calculated using mixing rules. The mixing rule for phase molar densities is

$$1/\rho_j = \sum_{i=1}^{N_c} (x_{ij}/\rho_{ij}) \tag{5}$$

where ρ_j represents the molar density of phase j in the mixed state, and ρ_{ij} represents the molar density of component i in phase j. The mixing rule for phase viscosities is

$$\ln\mu_j = \sum_{i=1}^{N_c} x_{ij} \ln\mu_{ij} \tag{6}$$

where μ_j represents the viscosity of phase j in the mixed state, and μ_{ij} represents the molar density of component i in phase j.

Fig. 10 presents the simulated cumulative production and daily production rate for the base and modified cases. The daily production for the modified case is consistently higher than that for

Table 10
Summary of the reservoir model used for the SAGD simulation case study.

Property	Value
Porosity	33%
Horizontal permeability	4000 md
Vertical permeability	3000 md
Initial reservoir pressure at depth of 500 m	15 bars
Initial reservoir temperature	286.15 K
Initial oil saturation	0.75
Initial water saturation	0.25
Three-phase relative permeability model (Computer Modelling Group, 2011)	Stone's model II
Formation compressibility	1.8E-05 1/kPa
Rock heat capacity (Keshavarz et al., 2014a)	2600 kJ/m^3 °C
Rock thermal conductivity (Keshavarz et al., 2014a)	660 kJ/m day °C
Over/underburden heat capacity (Keshavarz et al., 2014a)	2600 kJ/m^3 °C
Over/underburden thermal conductivity (Keshavarz et al., 2014a)	660 kJ/m day °C
Bitumen thermal conductivity	11.5 kJ/m day °C
Gas thermal conductivity	2.89 kJ/m day °C
Water thermal conductivity	150 kJ/m day °C
Bitumen molecular weight (Mehrotra and Svrcek, 1987)	594.60 g/mole
Bitumen molecular specific gravity (Mehrotra and Svrcek, 1987)	1.077
Injector bottom-hole pressure (maximum)	40 bars
Producer bottom-hole pressure (minimum)	15 bars
Producer steam flow rate (maximum)	1 m^3/day
Steam quality	0.9

the base case up to approximately 1000 days. Beyond this time, the production rate is lower for the modified case because the SAGD chamber has already reached the outer boundary of the reservoir model. For the first year, for example, the cumulative productions for the base and modified cases are 1939.00 m^3 and 2561.60 m^3, respectively. The cumulative production for the modified case is higher than that for the base case by 36.75% for the first year. The instantaneous production rates at 365 days are 8.81 m^3/day for the base case and 10.80 m^3/day for the modified case; that is, the modified case results in 22.59% higher production rate at 365 days.

The underlying mechanisms for the observed increase in oil production rate due to x_{wL} are examined by use of an analytical theory for SAGD oil production. On the basis of Reis (1992), Keshavarz et al. (2015) presented

$$q = \sqrt{0.5k\varphi g\Delta S_L \int_0^H (\alpha UI/\varepsilon)dz}, \tag{7}$$

where q is the volumetric drainage rate of the C_D component, k is the absolute permeability, φ is the porosity, g is the gravitational constant, ΔS_L is the difference between the initial and residual bitumen saturations, H is the reservoir thickness above the production well, z is the elevation from the production well, α is the thermal diffusivity of the reservoir, U is the chamber-interface velocity, ε is Reis' empirical factor for the temperature distribution beyond the chamber edge. The parameter "I" in Equation (7) is

$$I = -(1/U)\int_{T_{edge}}^{T_R} [M_{rL}MW_L\rho_L C_{C_DL}/(T - T_R)]dT, \tag{8}$$

where T_R is the original reservoir temperature, and T_{edge} is the chamber-edge temperature. M_{rL} is the L-phase relative mobility k_{rL}/μ_L, where k_{rL} and μ_L are the relative permeability and viscosity of the L phase, respectively. MW_L and ρ_L are the molecular weight and molar density of the L phase, respectively. C_{C_DL} is the volume fraction of the C_D component in the L phase. A derivation of Equation (7) was presented in Keshavarz et al. (2015), and is not duplicated here.

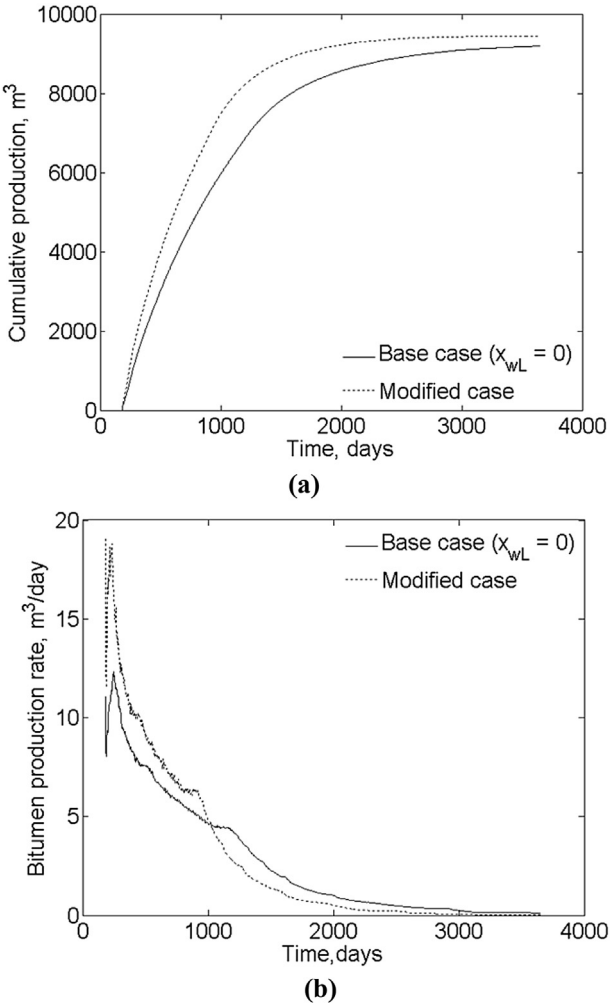

Fig. 10. SAGD simulation results. (a) Cumulative bitumen production for the base and modified cases. (b) Instantaneous production rate for the base and modified cases. For the modified case, the SAGD chamber reaches the outer boundary of the reservoir model within 1000 days. Beyond this time period, the production rate for the modified case is lower than that for the base case.

Although Equation (7) is based on various simplifying assumptions, such as constant temperature along the SAGD chamber edge, it clarifies that q can be affected by x_{wL} through M_{rL}, MW_L, ρ_L, and C_{C_DL}. The two cases exhibited only small differences in mass density ($MW_L\rho_L$), C_{C_DL}, temperature, and V-phase composition for a specified location relative to the chamber edge.

In the vicinity of the chamber edge, x_{wL} was observed to be higher than 30 mol% in the modified case. Fig. 11 compares the L-phase mobilities (kM_{rL}) for the base and modified cases for the 14th row from the top of the reservoir model at 365 days. It clearly shows that the dissolved water in the L phase increases the L-phase mobility. The effect of x_{wL} on bitumen-drainage rate is significant near the chamber edge. This is because x_{wL} increases with increasing temperature for a given oil and pressure, as discussed previously. For the same reason, SAGD at a higher operating pressure, which results in a higher operating temperature, exhibits more significant effect of x_{wL} on bitumen drainage. Also, reservoir heterogeneity will affect temperature distribution in a reservoir, which in turn will affect x_{wL}.

The analysis presented in this section is based on the simulation formulation in STARS (e.g., the mixing rules given in Equations (5) and (6)). It is recommended that bitumen–water interaction be properly considered in SAGD simulation with experimental data for x_{wL}, ρ_L, and μ_L for water-containing bitumen at elevated temperatures. The characterization method proposed in Section 2.4 can be used with at least one measured x_{wL} for reliable compositional phase-behavior predictions.

4. Conclusions

This research presented a reliable method for characterizing multiphase behavior of water-containing reservoir oil for steam injection simulation. The PR EOS with the van der Waals mixing rules was used. A new correlation was developed for BIPs for water with n-alkanes on the basis of the three-phase curves, including UCEPs, measured for water with n-alkanes by Brunner (1990). The BIP correlation developed for water/n-alkanes was subsequently applied to characterization of water-containing reservoir oil as the well-defined upper bound for BIPs for water/pseudo-components. The importance of properly considering x_{wL} in simulation of thermal bitumen recovery in SAGD was presented for the first time. Conclusions are as follows:

1. The PR EOS with the new BIP correlation can accurately represent three-phase curves measured by Brunner (1990) for water with n-alkanes. Type IIIa is predicted for water with n-alkanes up to n-C_{25}, and type IIIb for water with n-C_{26} and heavier. This transition between types IIIa and IIIb is plausible. Although the phase behavior classification was not clear for water with n-C_{26} and n-C_{27} in Brunner's experiments, he observed type IIIa for water with n-alkanes up to n-C_{25} and type IIIb for water with n-C_{28} and heavier.
2. The PR EOS with the new BIP correlation yields reasonable predictions of x_{wL} for water with n-alkanes up to n-C_{20}, for which limited experimental data are available in the literature. The PR EOS with the new BIP correlation reproduces the asymptotic behavior experimentally observed for three-phase curves and x_{wL} for water with heavy n-alkanes. As n-alkane becomes heavier, the three-phase curve approaches a certain asymptotic limit near the water vapor pressure curve in P–T space. The x_{wL} exhibits a limiting trend line in temperature that is nearly independent of n-alkane CN as long as temperature is not close to the UCEP temperature. A constant BIP of 0.242 is required for water with n-C_{26} and heavier when used with the PR EOS.
3. The BIP correlation gives the well-defined upper bound for BIPs of water with hydrocarbon components when matching x_{wL} for water-containing reservoir oil. Accurate x_{wL} predictions for bitumens were obtained by systematically reducing the BIP values from the developed correlation.
4. Bitumen recovery in SAGD can be substantially affected by x_{wL}. In the simulation case study conducted for an Athabasca bitumen at 40 bars, bitumen recovery for the first year was predicted to be approximately 37% higher when x_{wL} was properly considered in the simulation. An analysis of simulation results through SAGD theory showed that the L-phase mobility was enhanced by the dissolved water near the chamber edge. It is recommended that bitumen–water interaction be properly considered in SAGD simulation with experimental data for water-containing bitumen at elevated temperatures. The characterization method proposed in Section 2.4 can be used with at least one measured x_{wL} for reliable compositional phase-behavior predictions.

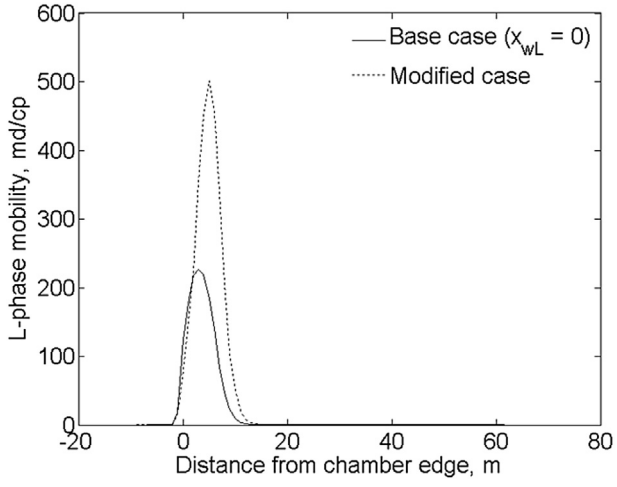

Fig. 11. L-phase mobility profile for the base and modified cases (SAGD) for the 14th row from the top at 365 days. The chamber-edge temperature for the base and modified cases are 507.64 K and 503.47 K, respectively. The temperature profiles for the base and modified cases do not differ significantly; for a specified location relative to the chamber edge, the temperatures for the two cases differ by less than 11 K. The difference in the L-phase mobility profile comes from x_{wL}.

Nomenclature

Roman symbols

C	volume fraction term in Equation (8)
$\Delta_m\underline{G}$	molar Gibbs free energy change on mixing
I	Integral term in Equation (7)
k	permeability, mD
L	oleic phase
M	mobility
P	pressure, bar
q	oil drainage rate
R	gas constant
S	saturation
T	temperature, K
U	velocity of condensation front
V	vapor phase
W	aqueous phase
x_{ij}	concentration of component i in phase j

Greek symbols

δ	distance in composition space
Δ	difference operator
λ	scaling factor for Equation (4)
μ	viscosity, cp
ρ	molar density, mol/m^3
ω	acentric factor

Subscripts

C	critical point
hc	hydrocarbon component
i	component index
j	phase index {L, V, W}
L	oleic phase
T	temperature
UCEP	upper critical endpoint
P	pressure
r	relative
V	vapor phase
w	water component
W	aqueous phase
3φ	three phases

Superscripts

base	base case
Data	values from measured data
EOS	values calculated from an EOS
mod	modified case

Abbreviations

AAD	absolute average deviation
AD	absolute deviation
^{o}API	American petroleum institute gravity
BIP	binary interaction parameter
CN	carbon number
EOS	equation of state
MW	molecular weight
UCEP	upper critical endpoint
PR	Peng and Robinson
PVT	pressure-volume-temperature

Appendix A. PR EOS with the van der Waals mixing rules

The PR EOS (Peng and Robinson, 1976a; Robinson and Peng, 1978) for a pure component is

$$P = \frac{RT}{\underline{V} - b} - \frac{a(T)}{\left(\underline{V}^2 + 2\underline{V}b - b^2\right)} \tag{A-1}$$

where a is the attraction parameter, b is the covolume parameter, R is the universal gas constant, and $\underline{V}$ is the molar volume. The attraction parameter is

$$a = 0.45724\frac{R^2T_c^2}{P_c}\alpha(T), \tag{A-2}$$

where α is the temperature dependence factor given as

$$\alpha(T) = \left(1.0 + m\left(1 - \sqrt{T_r}\right)\right)^2 \tag{A-3}$$

$$m = 0.37464 + 1.54226\omega - 0.26992\omega; \quad \omega \le 0.49 \tag{A-4}$$

$$m = 0.379642 + 1.48503\omega - 0.1664423\omega^2 + 0.01666\omega^3; \quad \omega > 0.49. \tag{A-5}$$

The covolume parameter is

$$b = 0.0778\frac{RT_c}{P_c}. \tag{A-6}$$

The van der Waals mixing rules are

$$a = \sum_{i=1}^{N_c}\sum_{j=1}^{N_c} x_i x_j \sqrt{a_i a_j}(1.0 - k_{ij}) \tag{A-7}$$

$$b = \sum_{i=1}^{N_c} x_i b_i, \tag{A-8}$$

where x_i is the mole fraction of component i in a mixture and k_{ij} is the BIP between components i and j.

Appendix B. Critical points and acentric factors for n-alkanes

The API technical data book (Daubert and Danner, 1997) gives recommended values for T_C, P_C, and ω for n-alkanes up to n-C_{30}. Kontogeorgis and Tassios (1997) presented a critical review for various estimation methods for T_C, P_C, and ω of heavy n-alkanes. They concluded that the group-contribution method of Constantinou and Gani (1994) and Constantinou et al. (1995) is reliable for the extrapolation to extended CNs. In this research, the values from the API technical data book (Daubert and Danner, 1997) and from the group contribution method (Constantinou and Gani, 1994; Constantinou et al., 1995) are integrated with smooth trends. The integration keeps the accuracy within the experimental uncertainties when measured values are available.

Table B-1 presents the integrated set of T_C, P_C, and ω for n-alkanes from C_1 to n-C_{100}. Available experimental data are also listed; the NIST Chemistry webbook (Linstrom and Mallard, 2001) is used for C_1 through n-C_4, and Nikitin et al. (1997) for n-C_5 through n-C_{36}. The T_C, P_C, and ω values given in Table B-1 are internally consistent in that Pitzer's definition of ω is satisfied when used with the PR EOS.

The values given in Table B-1 are correlated with the following equations:

$$T_C = 1410.705429[\ln(CN + 2.203385)]^{0.332560} - 1293.54872 \tag{B-1}$$

$$P_C = 46.83909\exp\left\{-0.5[\ln(CN/1.47310)/1.45642]^2\right\} + 1.31706 \tag{B-2}$$

$$\omega = 0.074020(CN)^{0.86699}\exp(-0.00245CN) - 0.04618 \tag{B-3}$$

The R^2 values are 0.9995, 0.9993, and 0.9999 for T_C, P_C, and ω, respectively. Maximum absolute deviations for T_C, P_C, and ω are 8.37 K for n-C_{24}, 1.58 bars for C_2, and 0.0120 for C_1. The standard deviation is 2.06 K for T_C, 0.206 bars for P_C, and 0.0024 for ω.

Table B-1
Critical constants and acentric factors for n-alkanes up to n-C_{100}. The integrated set is based on the API technical data book (Daubert and Danner, 1997), Constantinou and Gani (1994) and Constantinou et al. (1995).

CN	Integrated set			Experimental data			
	T_c, K	P_c, bar	ω	T_c, K	P_c, bar	Uncertainty in T_c, K	Uncertainty in P_c, bar
1	190.56	45.99	0.0157	190.60	46.10	0.30	0.30
2	305.32	48.72	0.0906	305.30	49.00	0.30	0.30
3	369.83	42.48	0.1543	369.82	42.50	0.20	0.10
4	425.12	37.96	0.2014	425.18	38.00	1.00	0.10
5	469.70	33.70	0.2511	469.70	33.70	0.20	0.67
6	507.60	30.25	0.3010	507.60	30.25	0.20	0.61
7	540.20	27.40	0.3505	540.20	27.40	0.30	0.55
8	568.70	24.92	0.3980	568.70	24.90	0.30	0.50
9	594.60	22.90	0.4459	594.60	22.90	0.60	0.46
10	617.70	21.10	0.4898	617.70	21.10	0.60	0.42
11	639.00	19.50	0.5306	639.00	19.80	1.00	0.40
12	658.00	18.20	0.5680	658.00	18.20	1.00	0.36
13	675.00	16.80	0.6077	675.00	16.80	1.00	0.34
14	693.00	15.70	0.6482	693.00	15.70	2.00	0.31
15	708.00	14.99	0.6896	708.00	14.80	2.00	0.30
16	723.00	14.14	0.7320	723.00	14.00	2.00	0.28
17	736.00	13.31	0.7753	736.00	13.40	2.00	0.27
18	747.00	12.51	0.8200	747.00	12.90	3.00	0.26
19	758.00	11.76	0.8634	755.00	11.60	8.00	0.23
20	768.00	11.05	0.9063	768.00	10.80	8.00	0.22
21	779.00	10.39	0.9430	778.00	10.30	8.00	0.21
22	788.00	9.77	0.9801	786.00	9.91	8.00	0.20
23	797.00	9.20	1.0168	790.00	9.15	8.00	0.18
24	806.00	8.88	1.0532	800.00	8.71	8.00	0.17
25	813.00	8.21	1.0894	–	–	–	–
26	820.23	7.79	1.1253	816.00	7.95	12.00	0.32
27	826.19	7.42	1.1609	–	–	–	–
28	831.85	7.29	1.1962	824.00	7.44	12.00	0.30
29	837.36	6.79	1.2312	–	–	–	–
30	842.67	6.52	1.2660	843.00	6.36	12.00	0.25
31	847.75	6.28	1.3004	–	–	–	–
32	852.63	6.07	1.3320	–	–	–	–
33	857.37	5.90	1.3665	–	–	–	–
34	862.01	5.75	1.4006	–	–	–	–
35	866.59	5.63	1.4344	–	–	–	–
36	871.16	5.53	1.4678	872.00	4.72	13.00	0.19
37	875.75	5.22	1.5008	–	–	–	–
38	880.38	5.07	1.5335	–	–	–	–
39	885.03	4.92	1.5659	–	–	–	–
40	889.67	4.78	1.5979	–	–	–	–
41	894.29	4.65	1.6296	–	–	–	–
42	898.90	4.53	1.6610	–	–	–	–
43	903.50	4.42	1.6921	–	–	–	–
44	907.59	4.31	1.7229	–	–	–	–
45	911.76	4.20	1.7533	–	–	–	–
46	915.83	4.11	1.7835	–	–	–	–
47	919.82	4.01	1.8134	–	–	–	–
48	923.72	3.92	1.8430	–	–	–	–
49	927.53	3.84	1.8724	–	–	–	–
50	931.27	3.76	1.9014	–	–	–	–
51	934.93	3.68	1.9302	–	–	–	–
52	938.52	3.61	1.9588	–	–	–	–
53	942.04	3.54	1.9870	–	–	–	–
54	945.49	3.48	2.0151	–	–	–	–
55	948.88	3.41	2.0429	–	–	–	–
56	952.21	3.35	2.0704	–	–	–	–
57	955.47	3.30	2.0977	–	–	–	–
58	958.68	3.24	2.1248	–	–	–	–
59	961.83	3.19	2.1516	–	–	–	–
60	964.93	3.14	2.1783	–	–	–	–
61	967.98	3.09	2.2047	–	–	–	–
62	970.97	3.04	2.2309	–	–	–	–
63	973.92	3.00	2.2568	–	–	–	–
64	976.82	2.95	2.2826	–	–	–	–
65	979.68	2.91	2.3082	–	–	–	–
66	982.49	2.87	2.3335	–	–	–	–
67	985.25	2.84	2.3587	–	–	–	–
68	987.98	2.80	2.3837	–	–	–	–
69	990.66	2.76	2.4085	–	–	–	–
70	993.31	2.73	2.4330	–	–	–	–
71	995.92	2.70	2.4575	–	–	–	–
72	998.49	2.66	2.4817	–	–	–	–

Table B-1 (*continued*)

CN	Integrated set			Experimental data			
	T_c, K	P_c, bar	ω	T_c, K	P_c, bar	Uncertainty in T_c, K	Uncertainty in P_c, bar
73	1001.02	2.63	2.5057	–	–	–	–
74	1003.52	2.60	2.5296	–	–	–	–
75	1005.99	2.58	2.5533	–	–	–	–
76	1008.42	2.55	2.5768	–	–	–	–
77	1010.82	2.52	2.6002	–	–	–	–
78	1013.19	2.50	2.6234	–	–	–	–
79	1015.53	2.47	2.6464	–	–	–	–
80	1017.84	2.45	2.6693	–	–	–	–
81	1020.12	2.42	2.6920	–	–	–	–
82	1022.37	2.40	2.7146	–	–	–	–
83	1024.59	2.38	2.7370	–	–	–	–
84	1026.79	2.36	2.7592	–	–	–	–
85	1028.96	2.34	2.7814	–	–	–	–
86	1031.10	2.32	2.8033	–	–	–	–
87	1033.22	2.30	2.8251	–	–	–	–
88	1035.32	2.28	2.8468	–	–	–	–
89	1037.39	2.26	2.8684	–	–	–	–
90	1039.43	2.25	2.8898	–	–	–	–
91	1041.46	2.23	2.9110	–	–	–	–
92	1043.46	2.21	2.9322	–	–	–	–
93	1045.44	2.20	2.9532	–	–	–	–
94	1047.40	2.18	2.9740	–	–	–	–
95	1049.34	2.16	2.9948	–	–	–	–
96	1051.26	2.15	3.0154	–	–	–	–
97	1053.15	2.14	3.0359	–	–	–	–
98	1055.03	2.12	3.0563	–	–	–	–
99	1056.89	2.11	3.0765	–	–	–	–
100	1058.73	2.10	3.0966	–	–	–	–

Appendix C. Supplementary data

Supplementary data related to this article can be found at http://dx.doi.org/10.1016/j.jngse.2015.07.036.

References

Ahmed, T., 2006. Reservoir Engineering Handbook. Gulf Professional Publishing.

Amani, M.J., Gray, M.R., Shaw, J.M., 2013a. Phase behavior of athabasca bitumen water mixtures at high temperature and pressure. J. Supercrit. Fluids 77, 142–152.

Amani, M.J., Gray, M.R., Shaw, J.M., 2013b. Volume of mixing and solubility of water in athabasca bitumen at high temperature and pressure. Fluid Phase Equilib. 358, 203–211.

Aparicio-Martínez, S., Hall, K.R., 2007. Phase equilibria in water containing binary systems from molecular based equations of state. Fluid Phase Equilib. 254 (1), 112–125.

Badamchi-Zadeh, A., Yarranton, H., Maini, B.B., Satyro, M., 2009. Phase behaviour and physical property measurements for VAPEX solvents: part II. Propane, carbon dioxide and athabasca bitumen. J. Can. Pet. Technol. 48 (3), 57–65.

Badamchi-Zadeh, A., Yarranton, H., Svrcek, W., Maini, B., 2009. Phase behaviour and physical property measurements for VAPEX solvents: part I. Propane and athabasca bitumen. J. Can. Pet. Technol. 48 (1), 54–61.

Barrufet, M.A., Liu, K., Rahman, S., Wu, C., 1996. Simultaneous vapor-liquid-liquid equilibria and phase molar densities of a quaternary system of propane + pentane + octane + water. J. Chem. Eng. Data 41 (4), 918–922.

Brunner, E., 1990. Fluid mixtures at high pressures IX. Phase separation and critical phenomena in 23 (n-alkane + water) mixtures. J. Chem. Thermodyn. 22 (4), 335–353.

Butler, R.M., 1994. Steam-assisted gravity drainage: concept, development, performance and future. J. Can. Pet. Technol. 33 (2), 44–50.

Butler, R.M., 2001. Some recent developments in SAGD. J. Can. Pet. Technol. 18–21.

Chawla, I.S., Barrufet, M.A., Rahman, S., Beladi, M.K., Wu, C.H., 1995. Influence of temperature, pressure and molecular weight of hydrocarbon components on the multi-phase equilibria of hydrocarbon/water systems. In: Presented at the SPE Annual Technical Conference and Exhibition, Dallas, U.S.A, 22–25 October.

Computer Modelling Group, 2011. STARS Version 2011 User Guide. CMG, Calgary, Alberta, Canada.

Constantinou, L., Gani, R., 1994. New group contribution method for estimating properties of pure compounds. AIChE J. 40 (10), 1697–1710.

Constantinou, L., Gani, R., O'Connell, J.P., 1995. Estimation of the acentric factor and the liquid molar volume at 298 K using a new group contribution method. Fluid Phase Equilib. 103 (1), 11–22.

Daridon, J.L., Lagourette, B., Saint-Guirons, H., Xans, P., 1993. A cubic equation of state model for phase equilibrium calculation of alkane + carbon dioxide + water using a group contribution k_{ij}. Fluid Phase Equilib. 91 (1), 31–54.

Daubert, T., Danner, R., 1997. API Technical Data Book-petroleum Refining. American Petroleum Institute (API), Washington DC.

Economou, I., Heidman, J., Tsonopoulos, C., Wilson, G., 1997. Mutual solubilities of hydrocarbons and Water: III. 1-Hexene, 1-octene, C_{10}–C_{12} hydrocarbons. AIChE J. 43 (2), 535–546.

Eubank, P.T., Wu, C.H., Alvarado, J.F., Forero, A., Beladi, M.K., 1994. Measurement and prediction of three-phase water/hydrocarbon equilibria. Fluid Phase Equilib. 102 (2), 181–203.

Glandt, C.A., Chapman, W.G., 1995. Effect of water dissolution on oil viscosity. SPE Reserv. Eng. 10 (1), 59–64.

Griswold, J., Kasch, J.E., 1942. Hydrocarbon-water solubilities at elevated temperatures and pressures. Ind. Eng. Chem. 34 (7), 804–806.

Heidemann, R.A., 1974. Three-phase equilibria using equations of state. AIChE J. 20 (5), 847–855.

Heidman, J.L., Tsonopoulos, C., Brady, C.J., Wilson, G.M., 1985. High-temperature mutual solubilities of hydrocarbons and water. Part II: ethylbenzene, ethylcyclohexane, and n-octane. AIChE J. 31 (3), 376–384.

Huron, M., Vidal, J., 1979. New mixing rules in simple equations of state for representing vapor-liquid equilibria of strongly non-ideal mixtures. Fluid Phase Equilib. 3 (4), 255–271.

Keshavarz, M., Okuno, R., Babadagli, T., 2014. Efficient oil displacement near the chamber edge in ES-SAGD. J. Pet. Sci. Eng. 118, 99–113.

Keshavarz, M., Okuno, R., Babadagli, T., 2014. Optimal application conditions for steam/solvent coinjection. SPE Reserv. Eval. Eng. 1–19.

Keshavarz, M., Okuno, R., Babadagli, T., 2015. A semi-analytical solution to optimize single-component solvent coinjection with steam during SAGD. Fuel 118, 400–414.

Kobayashi, R., Katz, D., 1953. Vapor-liquid equilibria for binary hydrocarbon-water systems. Ind. Eng. Chem. 45 (2), 440–446.

Kontogeorgis, G.M., Tassios, D.P., 1997. Critical constants and acentric factors for long-chain alkanes suitable for corresponding states applications. A critical review. Chem. Eng. J. 66 (1), 35–49.

Kumar, A., Okuno, R., 2013. Characterization of reservoir fluids using an EOS based on perturbation from n-alkanes. Fluid Phase Equilib. 358, 250–271.

Kumar, A., Okuno, R., 2014. Reservoir oil characterization for compositional simulation of solvent injection processes. Ind. Eng. Chem. Res. 53, 440–455.

Lake, L.W., 1989. Enhanced Oil Recovery. Prentice-Hall, Old Tappan, New Jersey.

Li, Y., Nghiem, L.X., 1986. Phase equilibria of oil, gas and water/brine mixtures from a cubic equation of state and Henry's law. Can. J. Chem. Eng. 64 (3), 486–496.

Linstrom, P.J., Mallard, W.G., 2001. NIST Standard Reference Database 69: Phase Change Properties. Standard Reference Data Program, National Institute of Standards and Technology, Gaithersburg, Maryland. http://webbook.nist.gov/chemistry (accessed 04.03.14.).

Luo, S., Barrufet, M.A., 2005. Reservoir simulation study of water-in-oil solubility effect on oil recovery in steam injection process. SPE Reserv. Eval. Eng. 8 (6), 528–533.

Maczynski, A., Shaw, D.G., Goral, M., et al., 2005. IUPAC-NIST solubility data series. 81. Hydrocarbons with water and seawater-revised and updated. Part 4. C_6H_{14} hydrocarbons with water. J. Phys. Chem. Ref. Data 34 (2), 709–753.
McKetta, J.J., Katz, D.L., 1948. Methane–n-butane–water system in two-and three-phase regions. Ind. Eng. Chem. 40 (5), 853–863.
Mehra, R.K., Heidemann, R.A., Aziz, K., 1982. Computation of multiphase equilibrium for compositional simulation. SPE J. 22 (1), 61–68.
Mehrotra, A.K., Svrcek, W.Y., 1985. Viscosity, density and gas solubility data for oil sand bitumens. Part II: peace river bitumen saturated with N_2, CO, CH_4, CO_2 and C_2H_6. AOSTRA J. Res. 1 (4), 269–279.
Mehrotra, A.K., Svrcek, W.Y., 1986. Viscosity of compressed athabasca bitumen. Can. J. Chem. Eng. 64, 844–847.
Mehrotra, A.K., Svrcek, W.Y., 1987. Corresponding states method for calculating bitumen viscosity. J. Can. Pet. Technol. 26 (5), 60–66.
Mohebbinia, S., Sepehrnoori, K., Johns, R.T., 2013. Four-phase equilibrium calculations of carbon dioxide/hydrocarbon/water systems with a reduced method. SPE J. 18 (5), 943–951.
Nasrifar, K., Moshfeghian, M., 2002. Liquid–liquid equilibria of water–hydrocarbon systems from cubic equations of state. Fluid Phase Equilib. 193 (1), 261–275.
Nikitin, E.D., Pavlov, P.A., Popov, A.P., 1997. Vapour-liquid critical temperatures and pressures of normal alkanes with from 19 to 36 carbon atoms, naphthalene and m-terphenyl determined by the pulse-heating technique. Fluid Phase Equilib. 141 (1), 155–164.
Olds, R.H., Sage, B.H., Lacey, W.N., 1942. Phase equilibria in hydrocarbon systems. Composition of the dew-point gas of the methane-water system. Ind. Eng. Chem. 34 (10), 1223–1227.
Pedersen, K.S., Christensen, P.L., Shaikh, J.A., 2006. Phase Behavior of Petroleum Reservoir Fluids. CRC Press, Boca Raton, Florida.
Peng, D.Y., Robinson, D.B., 1976. A new two-constant equation of state. Ind. Eng. Chem. Fundam. 15 (1), 59–64.
Peng, D., Robinson, D.B., 1976. Two and three phase equilibrium calculations for systems containing water. Can. J. Chem. Eng. 54 (5), 595–599.
Prats, M., 1982. Thermal Recovery. HL Doherty Memorial Fund of AIME, SPE, New York:
Reamer, H.H., Olds, R.H., Sage, B.H., Lacey, W.N., 1943. Phase equilibria in hydrocarbon systems. Composition of dew-point gas in ethane-water system. Ind. Eng. Chem. 35 (7), 790–793.
Reamer, H.H., Olds, R.H., Sage, B.H., Lacey, W.N., 1944. Phase equilibria in hydrocarbon systems. n-Butane–water system in three-phase region. Ind. Eng. Chem. 36 (4), 381–383.
Reis, J.C., 1992. A steam-assisted gravity drainage model for tar sands: linear geometry. J. Can. Pet. Technol. 31 (10), 14–20.
Robinson, D.B., Peng, D.Y., 1978. The Characterization of the Heptanes and Heavier Fractions for the GPA Peng-Robinson Programs. Gas Processors Association Research Report RR-28.
Satyro, M.A., Shaw, J.M., Yarranton, H.W., 2013. A practical method for the estimation of oil and water mutual solubilities. Fluid Phase Equilib. 355, 12–25.
Shaw, D.G., Maczynski, A., Goral, M., et al., 2005. IUPAC-NIST solubility data series. 81. Hydrocarbons with water and seawater- revised and updated. Part 7. C_8H_{12}–C_8H_{18} hydrocarbons with water. J. Phys. Chem. Ref. Data 34 (4), 2261–2298.
Shaw, D.G., Maczynski, A., Goral, M., et al., 2006a. IUPAC-NIST solubility data series. 81. Hydrocarbons with water and seawater-revised and updated. Part 9. C_{10} hydrocarbons with water. J. Phys. Chem. Ref. Data 35 (1), 93–151.
Shaw, D.G., Maczynski, A., Goral, M., et al., 2006b. IUPAC-NIST solubility data series. 81. Hydrocarbons with water and seawater-revised and updated. Part 11. C_{13}–C_{36} hydrocarbons with water. J. Phys. Chem. Ref. Data 35 (2), 687–784.
Shinta, A.A., Firoozabadi, A., 1997. Predicting phase behavior of water/reservoir-crude systems with the association concept. SPE Reserv. Eng. 12 (2), 131–137.
Skripka, V.G., 1979. Solubility of water in normal alkanes at elevated temperatures and pressures. Chem. Technol. Fuels Oils 15 (2), 88–90.
Søreide, I., Whitson, C.H., 1992. Peng-Robinson predictions for hydrocarbons, CO_2, N_2, and H_2S with pure water and NaCl brine. Fluid Phase Equilib. 77, 217–240.
Tsonopoulos, C., 1999. Thermodynamic analysis of the mutual solubilities of normal alkanes and water. Fluid Phase Equilib. 156 (1), 21–33.
Tsonopoulos, C., Heidman, J.L., 1986. High-pressure vapor-liquid equilibria with cubic equations of state. Fluid Phase Equilib. 29, 391–414.
Tsonopoulos, C., Wilson, G.M., 1983. High-temperature mutual solubilities of hydrocarbons and water. Part I: benzene, cyclohexane and n-hexane. AIChE J. 29, 990–999.
Wagner, W., Pruß, A., 2002. The IAPWS formulation 1995 for the thermodynamic properties of ordinary water substance for general and scientific use. J. Phys. Chem. Ref. Data 31 (2), 387–535.
Whitson, C.H., Brulé, M.R., 2000. Phase Behavior. HL Doherty Memorial Fund of AIME, SPE, Richardson, Texas.